Received: 11 February 2020 | Revised: 27 July 2021 | Accepted: 11 October 2021

DOI: 10.1002/rnc.5861

RESEARCH ARTICLE

WILEY

A QFT approach to robust dual-rate control systems

Alfonso Baños[1] | **Julián Salt**[2] | **Vicente Casanova**[2]

[1]Departamento Informática y Sistemas, Universidad de Murcia, Murcia, Spain

[2]Departamento Ingeniería de Sistemas y Automática, Universidad Politécnica de Valencia, Valencia, Spain

Correspondence
Alfonso Baños, Facultad de Informática, Universidad de Murcia, 30100 Murcia, Spain.
Email: abanos@um.es

Funding information
Fundación Séneca, Grant/Award Number: 20842/PI/18; MCIN/AEI/10.13039/501100011033 and "ERDF A way of making Europe", Grant/Award Numbers: PID2020-112709RB-C22, RTI2018-096590-B-I00

Abstract

A dual-rate control system is a hybrid system composed of continuous-time and discrete-time elements with two sampling frequencies. In this work, a new frequency domain analysis and design approach, based on the quantitative feedback theory is developed, to cope with robust stability and robust tracking specifications. Tracking specifications are considered not only in the discrete-time but also in continuous-time, that allow a precise description of the intersample behavior (ripples), and characterization of frequencies below and beyond the Nyquist frequencies. Several illustrative examples and a case study has been developed.

KEYWORDS

dual-rate control systems, frequency domain, multirate control systems, quantitative feedback theory, robust control

1 | INTRODUCTION

A multirate (MR) control system is defined as a hybrid system composed of continuous-time and discrete-time elements (plant, controllers, and filters), where two or more variables are sampled or updated at different frequencies.[1-3] Since many years ago these systems have been considered in industrial environments where chemical analyzers are needed,[4,5] or in visual feedback applications in robotics;[6,7] in all these cases post-processing requirements need a time interval that for a real-time process control request could be long. With these restrictions is not viable to keep and ideal single frequency in the control loop. In the last years, remote trajectory control of autonomous vehicles[8,9] and efficient energy saving in networked based control systems[10-12] also required the use of MR systems. In every these cases, the control problem is that with the mentioned restricted frequency of measurement, far away from the ideal one, is not possible to assure the correct performance of the system. MR control systems allow to achieve a performance close to the projected one with no frequency restrictions. A dual-rate (DR) system is a MR system where there are only two sampling frequencies. The case with slow output and fast input called MRIC (multirate input control) is especially important. In a DR system it is usual to consider an integer relation between the sampling periods and without jitter between both sequences. Different control design methods have been introduced for these kind of systems.[13-15] A big number of these contributions were inspired in classical time-domain or state-space approach single rate methods. It was also introduced the optimal H^∞ design in frequency domain[16,17] for MR systems but an iterative problem was the ripple of the system response. Some authors faced the robust control problem for MR systems.[18,19] Nevertheless there was not a frequency-based analysis or design method

inspired in classical techniques and, even more, assuming robust control. There was an inherent difficulty due to the complexity of the MR frequency response. In recent years, some contributions allow to make easier those purposes.[20-23]

In this work, the quantitative feedback theory (QFT)[24] is postulated as an efficient technique for analysis and design of DR control systems, including system with potentially large uncertainty. Being a sound and well-developed frequency domain technique, it is believed that QFT will be a unique framework for understanding how slow and fast sampling from the DR controller interact with the plant continuous dynamics, being a goal the efficient characterization of ripples and their removal with a proper controller design. QFT dates back to the seminal works of Isaac Horowitz[25] in the late fifties of the past century, that pioneered the analysis and design of linear and time-invariant systems with large uncertainty.[26] Although somehow aside of the mainstream robust control research, over the years QFT has been extended to cope with uncertainty in linear and time-varying systems,[27] nonlinear systems,[28-30] systems with multiple-input multiple-outputs,[31,32] multiloop,[24,33] and so forth, and has been also successfully applied in practice.[34] Specifically regarding (single-rate) sampled-data control systems, several QFT approaches have been developed. The classical approach is based on the application of continuous-time QFT through the use of the w-domain with the bilinear transformation.[35] A much more solid approach[36] includes continuous-time tracking and gain and phase margin problems, in line with several other works[37,38] that focus on the continuous-time response of a continuous plant under sampled data control, and has been a clear inspiration for this work.

The main contribution of this work is the development of a QFT framework for DR control systems having plants with potentially large uncertainty. It is mainly focused on the problem of robust stability and continuous-time tracking, and uses the slow-rate controller as design element. Several others performance specifications like disturbance rejection may be considered by using the developed framework. Some specific contributions are:

- The quantification of the closed-loop continuous-time response in the frequency domain under DR control, that will allow the efficient characterization of ripples, and in general of a desired intersample behavior.
- A Nyquist-like theorem for the robust stability of DR control systems, and the formulation of worst-case gain and phase margins, that results in QFT boundaries for the nominal slow open-loop gain function.
- Formulation of continuous-time tracking restrictions as QFT boundaries for the nominal slow open-loop gain function, for a given fast-rate controller and prefilter, with performance specifications below and beyond the slow Nyquist frequency.

As a result of the proposed approach, a number of new boundaries are developed that guaranty robust stability and continuous-time tracking. The next design steps are standard in QFT and will not be developed here in detail. Templates and boundaries computation is well-developed (note that only boundaries will be shown in the different examples along this work). The nominal open-loop gain shaping may be manually performed in simple cases, eventually with the aid of some computer toolbox.[39-42] Additionally, automatic loop-shaping techniques are also available.[43-46]

It is worthwhile to mention that the proposed QFT approach can be also applied to design single-rate controllers with continuous-time specifications beyond the Nyquist frequency, extending previous work[36] that suffered from that limitation. Also, it is useful for analyzing and designing DR controllers for plants with small or no uncertainty, although it is full potential is clearly obtained for the case of large uncertainty.

In Section 2, besides some basic preliminary results the DR control problem is formulated. Section 3 is about analysis of DR control systems in the frequency domain; first, a motivational example is investigated by using several analysis tools available in the literature, then new frequency-domain tools are proposed. As a result, a Nyquist-like theorem for exponential and L_p-stability of the DR control system is developed. Also, properties of the continuous-time signal spectra are derived that will be the basis for QFT approach to be developed in Section 4. Here, with the focus on robust stability and tracking (including continuous-time tracking), a detailed QFT-based method is formulated to solve the DR control problem, for systems with potentially large uncertainty. Finally, Section 5 is devoted to a case study for a reaction wheel inverted pendulum.

Notation: $\mathbb{R}_{\geq 0}$ is the set of non-negative real numbers, $\mathrm{L}_{pe}(\mathbb{R}_{\geq 0})$, or simply L_{pe}, is the extended space of $\mathrm{L}_p(\mathbb{R}_{\geq 0})$ (or simply L_p), which is the normed space of Lebesgue measurable functions $f : \mathbb{R}_{\geq 0} \to \mathbb{R}$ with $\|f\| = (\int_0^\infty |f(t)|^p dt)^{1/p} < \infty$ for $1 \leq p < \infty$, and $\|f\| = \text{ess sup}_{t \in \mathbb{R}_{\geq 0}} |f(t)|$ for $p = \infty$. For a function f of bounded variation on (a, b), $f(t^+) = \lim_{\varepsilon \to 0, \varepsilon > 0} f(t + \varepsilon)$, and $f(t^-) = \lim_{\varepsilon \to 0, \varepsilon > 0} f(t - \varepsilon)$, for any $t \in (a, b)$. For a dual-rate system with sampling periods $T_f, T_s \in \mathbb{R}$, and $T_f = T_s/N$, with a integer $N > 0$, the complex z-variables are $z_f = z$ and $z_s = z^N$. $\mathbb{C}$ is the set of complex numbers, $\mathbb{D} \subset \mathbb{C}$ is the open unit disk, and $\mathbb{D}^c = \mathbb{C} \setminus \mathbb{D}$, where $\setminus$ stands for set difference.

2 | PRELIMINARIES AND PROBLEM STATEMENT

For a continuous-time signal $x : \mathbb{R}_{\geq 0} \to \mathbb{R}$ and a sampling time T, a sampler S_T is a system that produces a sampled-data signal $x^T = S_T x : \mathbb{N}_{\geq 0} \to \mathbb{R}$, given by $x^T(n) = x(nT)$ for $n \in \mathbb{N}_{\geq 0}$. As it is well known,[47] if x is a function of bounded variation in every finite interval of $\mathbb{R}_{\geq 0}$, then the spectra of the signals x and x^T are related by (strictly speaking, x must also have a Laplace transform with abcissa of convergence $\sigma < 0$):

$$X^T(e^{j\omega T}) = \frac{x(0^+)}{2} + \sum_{k=1}^{\infty} \frac{x(kT^+) - x(kT^-)}{2} e^{-j\omega kT} + \frac{1}{T} \sum_{n=-\infty}^{\infty} X\left(j\left(\omega + n\frac{2\pi}{T}\right)\right) \tag{1}$$

where $\omega \in (-\infty, \infty)$. Obviously, if x is a continuous function over $\mathbb{R}_{\geq 0}$, and $x(0) = 0$, then the usual expression $X^T(j\omega) = \frac{1}{T}\sum_{n=-\infty}^{\infty} X\left(j\left(\omega + n\frac{2\pi}{T}\right)\right)$ is recovered.

On the other hand, a zero-order hold H_T, with sampling time T, is a system that acts over a discrete-time signal x^T and produces a continuous-time signal $x = H_T x^T$ given by $x(t) = x^T(n)$ for $nT \leq t < (n+1)T$ and $n \in \mathbb{N}_{\geq 0}$. In addition, and with some abuse of notation, the zero-order hold can be characterized by the function

$$H_T(j\omega) = \frac{1 - e^{-j\omega T}}{j\omega} \tag{2}$$

and the spectra of the signals x and x^T are related simply by $X(j\omega) = H_T(j\omega)X^T(e^{j\omega T})$.

Consider the DR control system of Figure 1 that will be the control setup to be investigated in this work, where all the signals are scalar. A continuous-time system, with transfer function $P(s)$, is controlled by a multirate controller working with two sampling periods T_s and T_f. It is assumed that $T_s \geq T_f$ and T_s will be referred to as the slow sampling time, and T_f as the fast sampling time. More specifically, the controller consists of two discrete-time controllers: a slow controller with two-degrees of freedom, with transfer functions $F_L(z_s)$ and $G_L(z_s)$, acting over signals sampled every T_s time units, and a fast controller $G_R(z_f)$, acting over signals sampled every T_f time units (note that the z-transform uses different values z_s or z_f to emphasize dependence on the sampling period T_s or T_f, respectively).

This work is focused on robust stability and tracking problems considering continuous-time responses. A previous QFT approach to sampled-data control[36] will be used as reference for approaching the QFT dual-rate control problem. More specifically the following closed-loop objectives are considered: robust stability with worst-case gain and phase margins, robust discrete-time tracking, and robust continuous-time tracking. A generic control design problem is: given a set of system transfer functions $\mathcal{P}$, and the prefilters $F(s)$ and $F_L(z_s)$, find discrete controllers $G_R(z_f)$ and $G_L(z_s)$ to meet the above objectives. Here, this problem is approached starting with a previously designed fast controller $G_R(z_f)$, thus the focus is on how to design the slow controller $G_L(z_s)$ to satisfy the closed-loop specifications. The z-transform of the slow

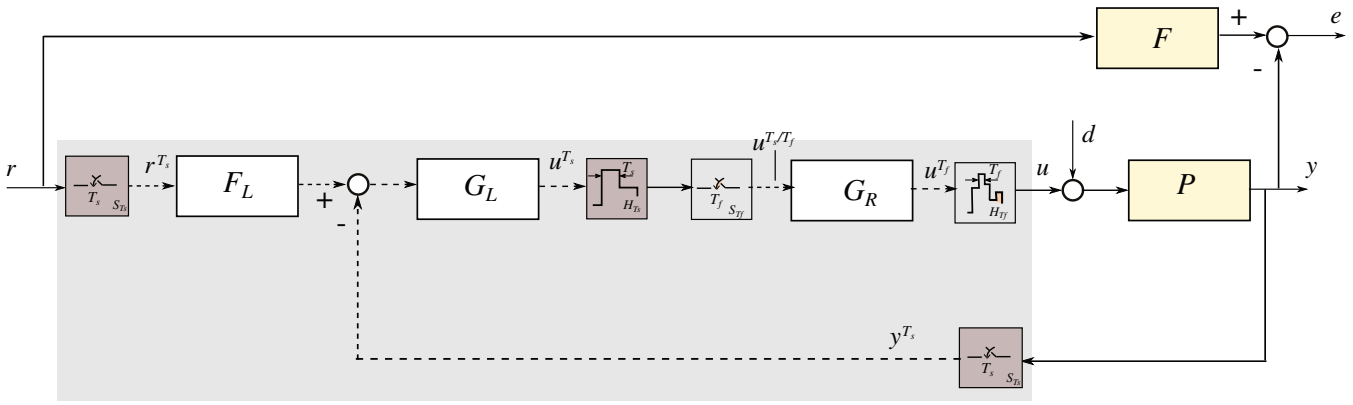

FIGURE 1 A dual-rate control system with discrete controllers G_R and (F_L, G_L) working at a fast/slow sampling time. The continuous system is given by a transfer function $P(s)$ in a set $\mathcal{P}$, the *slow* discrete controller is a two degrees of freedom controller with a prefilter $F_L(z_s)$ and a feedback controller $G_L(z_s)$, and its output is processed by a zero-order hold H_{T_s} followed by a sampler S_{T_f} before entering the *fast* discrete controller $G_R(z_f)$, being its output finally processed by a zero-order hold H_{T_f} to obtain the control input. Solid arrows correspond to continuous time signals, and dashed arrows to discrete time signals

controller output u^{T_s} is given by:

$$U^{T_s}(z_s) = G_L(z_s)(F_L(z_s)R^{T_s}(z_s) - Y^{T_s}(z_s)) \tag{3}$$

where, in addition, the continuous-time error signal e has the s-transform

$$E(s) = F(s)R(s) - Y(s) \tag{4}$$

and thus $U^{T_s}(z_s) = G_L(z_S)(E^{T_s}(z_s))$, once that $F_L(z_s) = \mathcal{Z}\{F(s)H_{T_s}(s)\}$. The output of the slow controller u^{T_s} is resampled with the fast sampling time obtaining the fast controller input u^{T_s/T_f}. This operation is modeled by using a combination of a zero-order hold H_{T_s} and a sampler with sampling time T_f. Finally, the output of the fast controller u^{T_f} is processed by a zero-order hold H_{T_f} producing the system input u. Note that in contrast to other QFT approaches based on tracking error specifications,[32,48,49] here the tracking specification is based on (4) and the continuous prefilter F and it is discretization F_L are first designed,[36] and then the emphasis will be on the design of the discrete feedback controller G_L for the continuous-time responses closely follow the response of the prefilter F.

It is also assumed that the exogenous signals and the system and controllers transfer functions satisfy the following standing assumption.

Assumption 1.

- The reference signal r and disturbance d are functions in $\mathrm{L}_{1e}(\mathbb{R}_{\geq 0})$ (signals in $\mathrm{L}_p(\mathbb{R}_{\geq 0})$, $1 \leq p \leq \infty$, such as steps, ramps, sinusoids, and so forth, are included; impulses are excluded).
- The system transfer function $P(s)$ is rational and strictly proper.
- The prefilter $F(s)$ is rational, strictly proper, and minimum-phase; and, in addition, the discrete prefilter $F_L(z_s)$ is the discretization of $F(s)$ as given by $F_L(z_s) = \mathcal{Z}\{F(s)H_{T_s}(s)\}$.
- The controllers $G_L(z_s)$ and $G_R(z_f)$ are rational and proper, and in addition $T_f = T_s/N$, that is $z_s = z_f^N$ (N is a positive integer). By notational simplicity $z = z_f$ and $z_s = z^N$ may be used.

3 | FREQUENCY DOMAIN ANALYSIS OF DUAL-RATE CONTROL SYSTEMS

Analysis of DR and in general MR sampled systems in the frequency domain has been developed since early contributions[20,22] to the field of digital control, trying to overcome the basic difficulty that multirate sampled systems are time-varying. In particular, several seminal works introduced switch decomposition[2,50] and frequency decomposition[51] techniques, that has been the basis for future developments. More recently, a relevant approach has been the lifting technique,[52,53] that transforms the periodic system into a linear time invariant one considering every signal referred to the least common multiple of all the periods of the MR system. The frequency domain analysis of multirate systems may be performed by using singular value decomposition (SVD) of the lifted MIMO system. Also, a number of works have extended the switch decomposition method of Kranc to very general cases obtaining which has been called a generalized Bode diagram (GBD).[54,55] By using a GBD, it is possible to analyze the several harmonic components of a DR sampled system as interleaved fragments of the frequency response of a particular single-rate system.

In the following, the lifted system SVD technique and, with some more detail, the GBD technique are applied to a DR control system to analyze its intersample behavior and motivate the QFT analysis and design technique to be developed in this work.

3.1 | A motivational example

Consider[56,57] the system with transfer function

$$P(s) = \frac{1.5}{(s + 0.5)(s + 1.5)} \tag{5}$$

and a DR controller with sampling times $T_s = 0.4$ s and $T_f = \frac{0.4}{3}$ s and thus $N = 3$, given by the slow and fast controllers (by simplicity a case without prefilter is analyzed, that is $F(s) = F_L(z^3) = 1$)

$$G_L(z^3) = \frac{z^9 - 1.296z^6 + 0.5636z^3 - 0.1721}{z^9 - 2.131z^6 + 1.365z^3 - 0.2344} \tag{6}$$

and

$$G_R(z) = \frac{26.31z^4 - 85.24z^3 + 102.1z^2 - 53.32z + 10.21}{z^4 - 1.469z^3 - 0.2344z^2 + 1.225z - 0.5089} \tag{7}$$

respectively. The goal of this DR controller is to emulate the design specifications obtained by the continuous-time PID controller $G_c(s) = 7.5\left(1 + 0.2s + \frac{1}{3s}\right)$, that will be used for comparison. It is desired that the DR controller achieves similar closed-loop performance but satisfying design implementation constraints such a slow output sampling and fast input sampling of the system (5). The reader is referred to References 56 and 57 for technical details about the DR controller computation.

A simulation of this DR control system has been performed, and results are shown in Figure 2. Although its performance in terms of unit step tracking seems to be correct in comparison with the PID controller, both at the slow and fast sampling periods (see Figure 2-left), the step response of the DR controller (see Figure 2-center) exhibits a ripple that degrades the intersample behavior and is clearly unacceptable in control practice. This ripple is obtained at a frequency $\omega_{ripple} = \frac{3\pi}{0.4} \approx 23.6$ Rad/s which is exactly the fast Nyquist frequency, that is $\omega_{ripple} = \frac{\pi}{T_f}$.

Now, the question is if some of the previously developed methods for frequency analysis is able to detect this intersample behavior in a efficient way. Figure 2-right shows both the (magnitude) GBD and SVD plots corresponding to the closed-loop system (reference to output), taking from References 56,57. Note that the oscillating intersampling behavior or ripple is due to the folding of high frequencies, and this alias at $\omega_{ripple} \approx 23.6$ Rad/s is barely distinguishable in the SVD diagram, that makes very difficult if not impossible to estimate the frequency and amplitude of the ripple using SVD. However, in the GBD both the ripple amplitude and frequency are clearly depicted. This is explained in detail in the following, discussing some limitations of the technique that has been a main motivation for this work.

The GBD technique[23] allows the computation of the frequency response from r^{T_s} to y^{Tf} (see Figure 1) by using only one Bode plot, and even for a more general case in which N_f and N_s are coprime integers (being $N_s T_s = N_f T_f$). It is understood that this "frequency response" does not give a single sinusoidal output for a sinusoidal input, in fact for a input $r^{T_s}(k) = e^{j\omega T_s k}$ the output is a sum of components $y_r(k) = \hat{y}_r e^{j\omega_r T_f k}$ with frequencies $\omega_r = \omega + r\frac{2\pi}{N_f T_f}$, $r = 0, 1, \ldots, N_f - 1$. And the GBD plot is used to compute $\hat{y}_r$ at the N_f frequency points ω_r, for $r = 0, 1, \ldots, N_f - 1$. Note that this technique only allows to analyze the frequencies appearing in the sampling of the signal of interest (in this case the output y^{Tf}). For

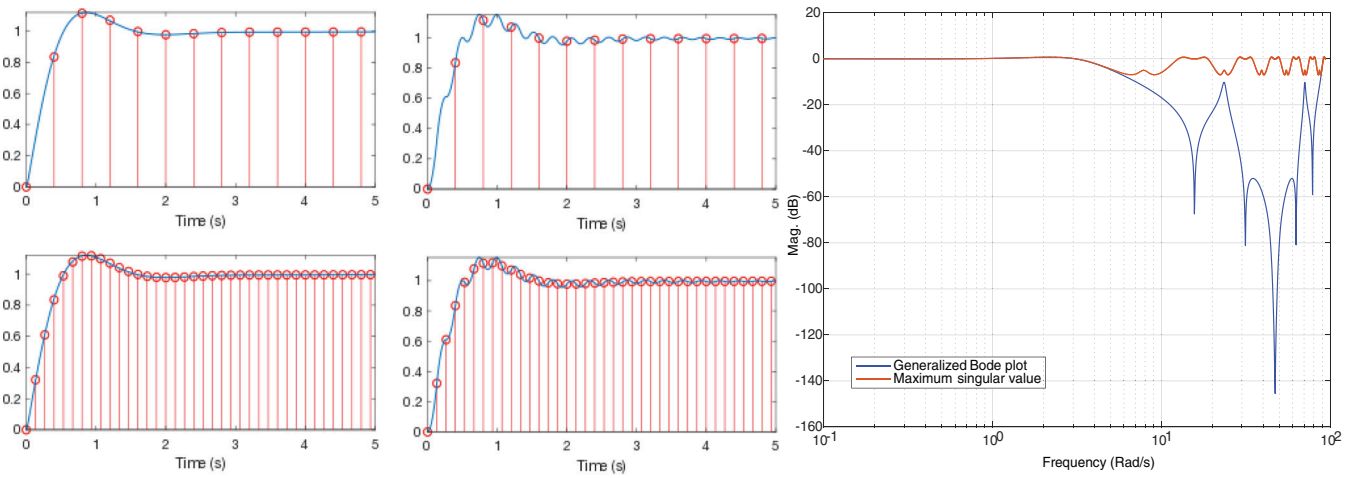

FIGURE 2 DR control system: (Left) Closed-loop step response of the PID controller and the DR controller at slow sampling -up- and at fast sampling -down-; (center) Closed-loop step response of the DR controller and their slow sampling -up- and fast sampling -down-; (right) Generalized Bode plot and maximum singular value versus frequency (closed-loop system)

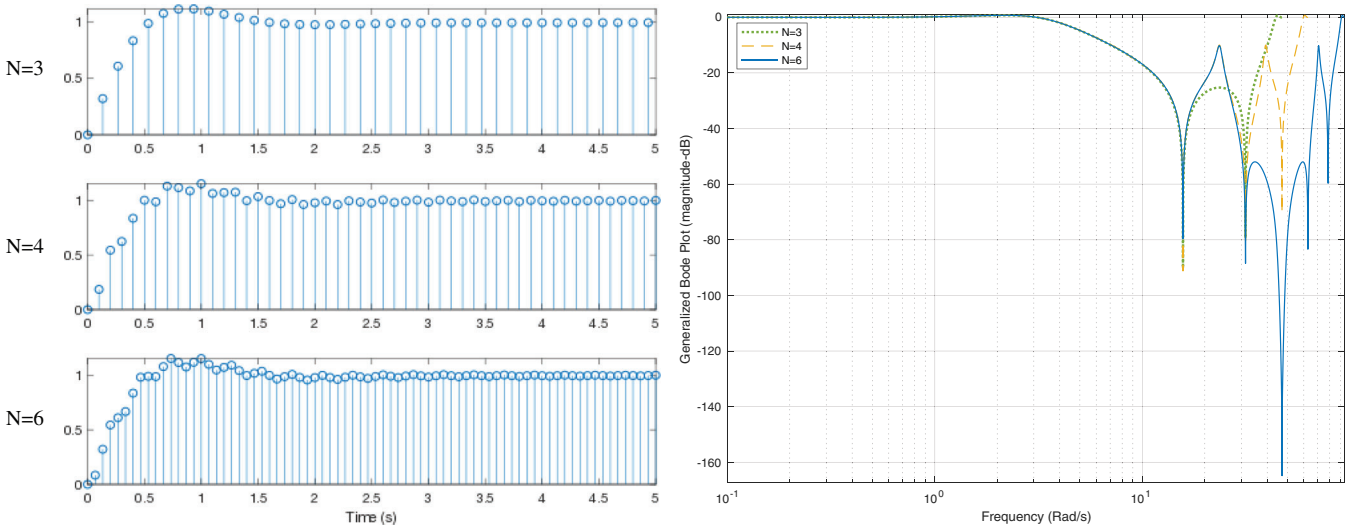

FIGURE 3 DR control system: (Left) Closed-loop step response of the DR controller at several sampling periods $T_f = T_s/N$, for $N = 3$, 4, and 6; (right) Generalized Bode plot for $N = 3$, 4, and 6 (note that the GBD plot of Figure 2-right corresponds to $N = 6$)

a finer intersample behavior analysis, the usual practice[58,59] is to sample the output at a faster sampling period and then to obtain the corresponding frequency components from the GBD.

For this example, and also in this work (see Assumption 1), $N_s = 1$ and $N_f = N$ which are clearly coprime, and thus the GBD can be applied. Figure 3 shows step responses and GBD plots of the DR control system example sampled at several sampling periods with $N = 3$, 4, and 6. Note that for $N = 3$, with Nyquist frequency $\omega_{Nyquist(N=3)} = \frac{3\pi}{0.4} \approx 23.56$ Rad/s, the GBP does have a relatively small value in magnitude, under -20 dB, for frequencies between approximately 1 and 23.56 Rad/s, and thus a ripple is not expected in the sampled signal as it is observed in the corresponding time response (Figure 3). However, for the case $N = 4$ with a frequency range $[0, \omega_{Nyquist(N=4)}] \approx [0, 31.42]$ Rad/s, the GBD clearly shows one (only) peak at the ripple frequency $\omega_{ripple} \approx 23.56$ Rad/s, that is also observed at the time response. Finally, for $N = 6$ with a frequency range $[0, \omega_{Nyquist(N=6)}] \approx [0, 47.12]$ Rad/s, the GBD only shows a significant peak at the frequency ω_{ripple}, clearly observed also in the time response.

Although the GBD technique allows the analysis of ripples occurrence, and in general frequency domain analysis of DR systems, a drawback is that it only allows the frequency analysis of the continuous-time signals of interest (like the control signal and the closed-loop output) in a somehow indirect way through their samples. Obviously, this can be partly alleviated by using a large value of N, but this is always an approximated analysis. Another more important issue that hampered the application of GBD in control practice, is that it is not obvious how to use GBD to design DR controllers, specially for systems with large uncertainty.

In the rest of this work, after developing a basic extension of the GBD technique to directly obtain continuous-time signal spectra, this result will be used as basis to develop a QFT-based methodology of robust DR controller design, that will be specially useful for systems with large uncertainty.

3.2 | A Nyquist-like theorem for nominal closed-loop stability

Before analyzing the frequency response of the DR control system, it is necessary to substantiate a stability result. By simplicity, the case of no uncertainty in P is considered here (robust stability is developed en Section 4.1). Also note that, by Assumption 1, $T_f = T$ and $T_s = NT$. The DR control system of Figure 1 is now modeled at different signal levels, from the continuous-time signals to the discrete-time signals given by the sampling with the fast and slow sampling periods. With some abuse of notation, the plant and the different controllers are now represented as time domain operators (see Figure 4): P is the continuous-time LTI plant, $P_R = S_T P H_T$ is its "fast" discretization (which is the zero-order hold equivalent of P at the fast sampling), and $K = H_T K_R S_T$ is a continuous-time controller, where K_R is a discrete-time controller with input and output y^{T_f} and u^{T_f}, respectively, given by $K_R = G_R Q_N^* G_L S_N$. Here, G_R and G_L are the fast and slow controllers, respectively, and S_N and Q_N^* will be defined in the following. Finally, $P_L = S_N P_R G_R Q_N^*$.

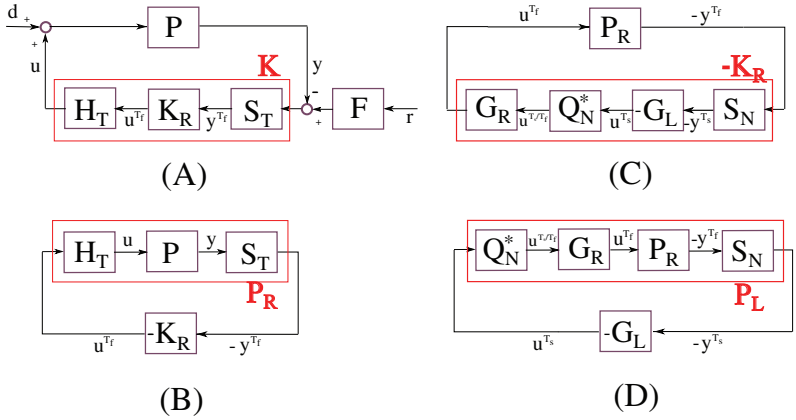

FIGURE 4 Representation of the DR control system as a feedback system interchanging different signals models: (A) Dual-rate system (P, K, F), with continuous-time signals u and y and exogenous signals r and d; the system (P, K) is obtained by doing $d = r = 0$; (B) Discrete-time system (P_R, K_R), with fast-sampled signals u^{T_f} and y^{T_f}, and internal signals u and y; (C) Discrete-time system (P_R, K_R) with several internal signals: slow-sampled signals u^{T_s} and y^{T_s} and the upsampled signal u^{T_s/T_f}; (D) Discrete-time system (P_L, G_L) with slow-sampled signals u^{T_s} and y^{T_s}, and internal signals u^{T_r}, y^{T_r}, and u^{T_s/T_f}

Here S_N is a sampler of a discrete-time signal x that gives the discrete-time signal $(S_N x)(k) = x(kN)$, for $k \geq 0$, and in the setup of Figure 1 $y^{T_f} = S_T y$ and $y^{T_s} = S_N y^{T_f} = S_N S_T y$ are obtained. Moreover Q_N^* represents the operation in Figure 1 corresponding to the zero-holding and resampling of u^{T_s} for obtaining u^{T_s/T_f}. Q_N^* has been referred to as a Q-upsampler[60] (with $Q = [1, 1, \ldots, 1]$) in contrast to the zero padding upsampler S_N^* (corresponding to $Q = [1, 0, \ldots, 0]$) used in previous seminal works,[37] which is the adjoint of S_N.

As a result, the DR control system of Figure 1 corresponds to (P, K, F) in Figure 4A. If exogenous inputs are not considered, that is $r = d = 0$, the autonomous DR control systems is denoted by (P, K). Moreover, (P_R, K_R) and (P_L, K_L) correspond to discrete-time models of (P, K) with fast and slow sampling, respectively (Figure 4B–D).

For the DR system (P, K), the state $\mathbf{x}(t) = (\mathbf{x}_P, \mathbf{x}_K)(t)$ is sufficient information for the computation of all future values of all signals[37] in the absence of exogenous inputs. By definition, (P, K) is exponentially stable if there exist positive constants α and β such that for every initial time t_0 and every initial state $\mathbf{x}(t_0)$, $\|\mathbf{x}(t)\| \leq \|\mathbf{x}(t_0)\| \beta e^{\alpha(t-t_0)}$. A similar definition can be stated in discrete-time for the feedback systems (P_R, K_R) and (P_L, K_L) in Figure 4. On the other hand, the DR system (P, K, F) is L_p-stable if the operators from d, r to e, u are bounded from L_p to L_p, for $1 \leq p \leq \infty$.

Consider the following standing assumption:

Assumption 2.

1. (Non-pathological fast sampling of the continuous-time plant) None of the points $jk\frac{2\pi}{T_f}$, $k \neq 0$ is a pole of P, and if s_p is a pole of P in CRHP then $s_p + jk\frac{2\pi}{T_f}$ is not a pole of P, for $k \neq 0$.
2. (Non-pathological slow sampling of the fast discrete-time plant) If z_p is a pole of P_R in $\mathbb{D}^c$ then $z_p e^{jk\frac{2\pi}{N}}$ is not a pole of P_R, for $k = 1, 2, \ldots, N-1$.
3. (No unstable hidden modes with fast and slow sampling) There is not pole-zero cancellations of the products $P_R G_R$ and $P_L G_L$ in $\mathbb{D}^c$.
4. (stability of the fast controller) The poles of G_R are in $\mathbb{D}$.

Since our approach is based on the frequency domain, a Nyquist-like theorem will be developed, adapting previous results[37,38,61,62] to our control setup. In the following, the full Nichols plot of $P_L \cdot G_L$ refers to the plot of $\left| P_L\left(e^{j\omega T_s}\right) \cdot G_L\left(e^{j\omega T_s}\right) \right|$ in dB against $\angle P_L\left(e^{j\omega T_s}\right) \cdot G_L(e^{j\omega T_s})$ in the domain $[-360, 0]$ degrees, for $\omega \in [0, 2\pi/T_s]$. Also the half Nichols plot corresponds to the segment of the full Nichols plot for $\omega \in [0, \pi/T_s]$. The next result is based on the number of crossings[61,62] of the full Nichols plot. Afterwards, the result is adapted to the half Nichols plot in a remark. In this work, for simplicity the half Nichols plot will be also referred to as the Nichols plot.

Proposition 1. *Under Assumptions 1 and 2, if in addition the full Nichols plot of $P_L \cdot G_L$ does not intersect the point $(-180°, 0\ \text{dB})$ and the net sum of crossings of the ray $\mathbf{R}_0 := \{(-180°, r) : r > 0\ \text{dB}\}$ is equal to the number of poles of $P_L \cdot G_L$*

(including multiplicities) in $\mathbb{D}^c$ (the crossing condition), then the DR control system (P, K) is exponentially stable and (P, K, F) is input-output L_p-stable, for $1 \leq p \leq \infty$.

Proof. First, consider the discrete-time feedback system (P_L, G_L) (Figure 4D). The system $P_L = S_N P_R G_R Q_N^*$ will be shown to be time-invariant. Before that, some properties of the upsampler Q_N^*, the backward shift U, and forward shift U^* need to be elaborated. It easily follows that

$$Q_N^* U = U^N Q_N^* \tag{8}$$

and

$$U^{*N} Q_N^* = Q_N^* U^* \tag{9}$$

Some other well-known properties[37] in relation with S_N, besides $S_N S_N^* = I$ and $U^* U = I$, are

$$U S_N = S_N U^N \tag{10}$$

and

$$U^* S_N = S_N U^{*N} \tag{11}$$

Also, a discrete-time linear system G is time-invariant if $U^* G U = G$, and is N-periodic if $U^{*N} G U^N = G$.
Now, from (10) to (11) it directly follows that

$$U^* P_L U = U^* S_N P_R G_R Q_N^* U = S_N U^{*N} P_R G_R U^N Q_N^* \tag{12}$$

In addition, by using the fact that G_R and P_R are time-invariant, and the identities (8)–(9), it results

$$U^* P_L U = S_N U^{*N} P_R G_R U^N Q_N^* = S_N P_R U^{*N} U^N G_R Q_N^* = P_L \tag{13}$$

that is, P_L is time-invariant. Since the full Nichols plot of $P_L \cdot G_L$ satisfies the crossing condition, it is a standard result[61,62] that (P_L, G_L) is exponentially stable.

Next, consider the stability of the discrete-time system (P_R, K_R) (Figure 4B,C). In contrast with the above reasoning, now K_R is not time-invariant. However, it will be shown that K_R is N-periodic. This directly follows by using (8)–(9) and the fact that G_R and G_L are time-invariant, that is

$$U^{*N} K_R U^N = U^{*N} G_R Q_N^* G_L S_N U^N = G_R U^{*N} Q_N^* G_L S_N U^N = G_R Q_N^* U^* G_L U S_N = G_R Q_N^* G_L S_N = K_R \tag{14}$$

And thus, all the conditions of Theorem 1[37] are satisfied (note that in this Theorem the zero padding upsampler S_N^* is used instead of the upsampler Q_N^*, and thus it is not directly applicable), and as a result the system (P_R, K_R) is exponentially stable. Finally, the exponential stability of the DR system (P, K) and the L_p-stability of the DR system (P, K, F) follows by direct application of Theorem 4[37] and Theorem 7,[38] respectively. ∎

Remark 1. Note that the ray crossings have a positive sign when the full Nichols plot crosses from left to right, and a negative sign in the opposite direction.[62] On the other hand, it is customary in QFT to work with the half Nichols plot (that will be referred to as Nichols plot in the rest of this work) of $P_L \cdot G_L$ as design element. Note that one crossing of the Nichols plot corresponds to two crossings of the full Nichols plot. In addition, some care with the crossings count is needed in the cases in which the Nichols plot starts or ends at the ray $\mathbf{R}_0$; in these cases, they should be counted as half crossings. Also, if there are poles of $P_L \cdot G_L$ in $z_s = 1$, there is a segment of the full Nichols plot from $\omega = 0^-$ to $\omega = 0^+$ (coming from the indentation of the Nyquist path at $z_s = 1$) that may produce crossings of $\mathbf{R}_0$: it counts as -1 crossing of the full Nichols plot and $-1/2$ crossing of the Nichols plot (see technical details in References 61,62).

Moreover, as it is well-known,[36] stability margins are conveniently depicted in the Nichols plane (see Figure 5): if $P_L\left(e^{j\omega T_s}\right) G_L\left(e^{j\omega T_s}\right) = l e^{\lambda}$ then the gain margin is defined as $\mathrm{GM} = 1/l$ at $\lambda = -180°$, and the phase margin is $\mathrm{PM} = 180° + \lambda$ where λ is the phase corresponding to $l = 1$.

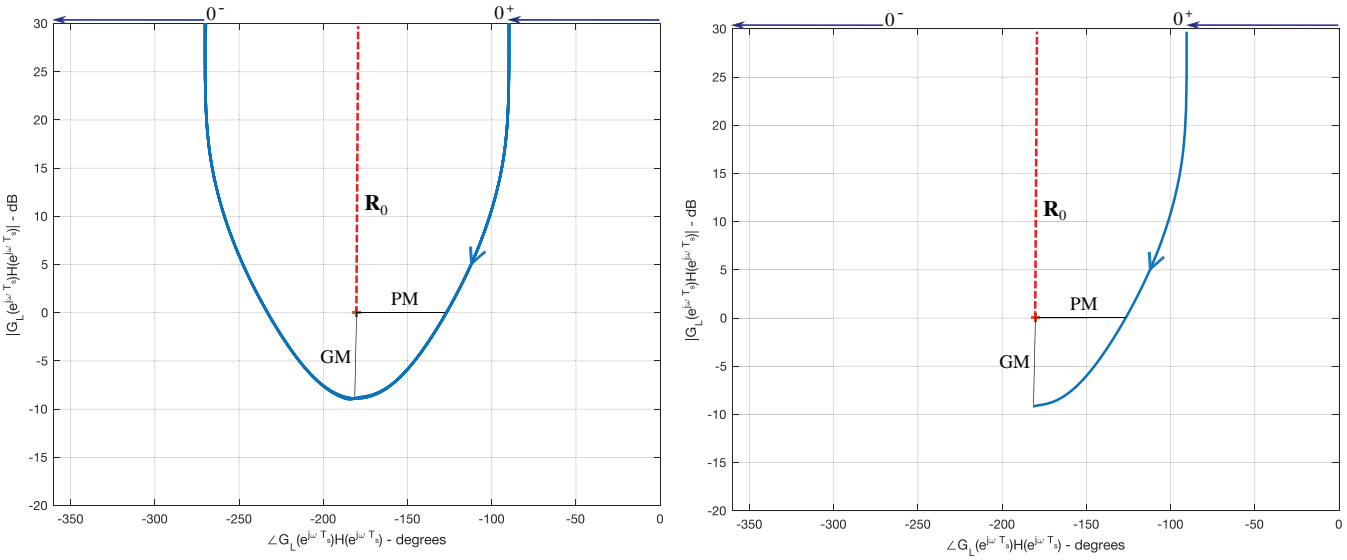

FIGURE 5 DR control system example of Section 3.1: Full Nichols plot (left) and Nichols plot (right) of $G_L \cdot P_L$, showing no crossings of the ray $\mathbf{R}_0$, and phase and gain margins

Example 1. Consider the example of Section 3.1. To apply the stability Nyquist result of Proposition 1, first Assumption 2 must be checked (Assumption 1 easily follows):

1. $P(s)$, given by (5), has real poles. Thus, fast sampling is non-pathological.
2. Here $P_R(z) = \frac{1.197e{-}05z{+}1.194e{-}05}{z^2{-}1.992z{+}0.992}$, having zeros and poles in $\mathbb{D}$. No unstable cancellation is possible.
3. Poles of $P_R(z)$ are real, and thus slow sampling is non-pathological.
4. Poles of $G_R(z)$, given by (7), are in $\mathbb{D}$.

Once it is shown that the Nyquist test can be applied, it has to be checked that there are no crossing of the full Nichols plot of $P_L \cdot G_L$ with the ray $\mathbf{R}_0$, since $(P_L \cdot G_L)(z^N)$ has no poles in $\mathbb{D}^c$. Figure 5 shows the full Nichols plot and the Nichols plot, and the fact that there are no crossings. As a result, exponential and L_p-stability of the DR control system directly follows.

3.3 | Continuous-time signals spectra in dual-rate systems

A basic goal of this work is to analyze, if possible, the frequency responses from the control system input r to signals of interest like the control input u and the output y. Besides stability, this work is specifically devoted to tracking problems, and thus it is consider $d = 0$ in the rest of this work (the case of non zero disturbances can be approached by using a similar treatment), that is $Y(s) = P(s)U(s)$. Thus, the key question is if it is possible to establish a frequency response that relates the reference input r to the output y. It will be shown that indeed it is possible, although with some limitation.

Consider the discrete sensitivity frequency response $S_L\left(e^{j\omega T_s}\right)$ defined as

$$S_L\left(e^{j\omega T_s}\right) = \frac{1}{1 + G_L\left(e^{j\omega T_s}\right) P_L\left(e^{j\omega T_s}\right)} \tag{15}$$

where $P_L\left(e^{j\omega T_s}\right)$ is the frequency response function corresponding to $P_L = S_N P_R G_R Q_N^*$, and the complementary sensitivity frequency response $T(j\omega)$ defined as

$$T(j\omega) = P(j\omega) G_R(e^{j\omega T_f}) H_{T_s}(j\omega) G_L\left(e^{j\omega T_s}\right) S_L\left(e^{j\omega T_s}\right) \tag{16}$$

Note that $T(j\omega)$ is not a sensitivity function in the conventional sense, here it is used to relate the spectrum of a slow sampled reference signal (discrete time) to the spectrum of the output signal (continuous time). This notation about sensitivity functions is common is sampled data systems[36,47]

The following result establishes the frequency responses from r^{T_s} to y^{T_s} and from r^{T_s} to y. The existence of the first frequency response, establishing the frequency response at the slow sampling time, is more or less obvious once the fast sampling time is a multiple of the slow sampling time. However, the existence of a (exact) frequency relationship between the sampled signal r^{T_s} and the continuous-time signal y is less evident.

Proposition 2. *Consider the DR control system of Figure 1, and assume that the stability conditions of Proposition 1 are satisfied. Then, for the case $Y(s) = P(s)U(s)$ ($d = 0$), the spectra of the system output y and its slow sampling y^{T_s} are given by*

$$Y(j\omega) = T(j\omega)F_L\left(e^{j\omega T_s}\right)R^{T_s}\left(e^{j\omega T_s}\right) \tag{17}$$

and

$$Y^{T_s}\left(e^{j\omega T_s}\right) = \left(1 - S_L\left(e^{j\omega T_s}\right)\right)F_L\left(e^{j\omega T_s}\right)R^{T_s}\left(e^{j\omega T_s}\right) \tag{18}$$

respectively.

Proof. Since, according to Assumption 1, P is a strictly proper rational function, then the spectrum of the slow sampled output y^{T_s} is directly given by

$$Y^{T_s}\left(e^{j\omega T_s}\right) = \frac{1}{T_s}\sum_{n=-\infty}^{\infty} Y\left(j\left(\omega + n\frac{2\pi}{T_s}\right)\right) \tag{19}$$

where the spectrum of y is

$$Y(j\omega) = P(j\omega)H_{T_f}(j\omega)U^{T_f}(e^{j\omega T_f}) \tag{20}$$

and, in addition,

$$U^{T_f}(e^{j\omega T_f}) = G_R(e^{j\omega T_f})U^{T_s/T_f}(j\omega) \tag{21}$$

Moreover, using (1), the fact that the signal $H_{T_s}(u^{T_s})$ is a function of bounded variation (but not necessarily continuous), and that the slow discrete controller is initially at rest, it follows that

$$U^{T_s/T_f}(j\omega) = \sum_{k=1}^{\infty}\frac{u_H(kT_f^+) - u_H(kT_f^-)}{2}e^{-j\omega kT_f} + \frac{1}{T_f}\sum_{n=-\infty}^{\infty} H_{T_s}\left(j\left(\omega + n\frac{2\pi}{T_f}\right)\right)U^{T_s}\left(e^{j\left(\omega + n\frac{2\pi}{T_f}\right)T_s}\right) \tag{22}$$

Now, since $T_s = NT_f$, the right-hand first and second terms of (22) can be simplified considering that

$$\sum_{k=1}^{\infty}\frac{u_H(kT_f^+) - u_H(kT_f^-)}{2}e^{-j\omega kT_f} = \sum_{k=1}^{\infty}\frac{u^{T_s}(k) - u^{T_s}(k-1)}{2}e^{-j\omega kT_s} = \frac{1 - e^{-j\omega T_s}}{2}U^{T_s}\left(e^{j\omega T_s}\right) \tag{23}$$

and

$$U^{T_s}\left(e^{j\left(\omega + n\frac{2\pi}{T_f}\right)T_s}\right) = U^{T_s}\left(e^{j(\omega T_s + n2\pi N)}\right) = U^{T_s}\left(e^{j\omega T_s}\right) \tag{24}$$

and also that

$$\frac{1 - e^{-j\omega T_s}}{2} + \frac{1}{T_f}\sum_{n=-\infty}^{\infty} H_{T_s}\left(j\left(\omega + n\frac{2\pi}{T_f}\right)\right) = \frac{1 - e^{-j\omega T_s}}{1 - e^{-j\omega T_f}} \tag{25}$$

Using (23), (24), and (25), the spectrum of the signal u^{T_s/T_f}, given by (22), is finally

$$U^{T_s/T_f}\left(e^{j\omega T_f}\right)=\left(\frac{1-e^{-j\omega NT_f}}{1-e^{-j\omega T_f}}\right)U^{T_s}\left(e^{j\omega NT_f}\right)=H_{T_s/T_f}\left(e^{j\omega T_f}\right)U^{T_s}\left(e^{j\omega NT_f}\right) \tag{26}$$

where $H_{T_s/T_f}(e^{j\omega T_f})$ corresponds to the frequency response of the upsampler Q_N^*. From (19), (20), (21), and (26) it is obtained

$$Y^{T_s}\left(e^{j\omega T_s}\right)=\frac{1}{T_s}\sum_{n=-\infty}^{\infty}P\left(j\left(\omega+n\frac{2\pi}{T_s}\right)\right)H_{T_f}\left(j\left(\omega+n\frac{2\pi}{T_s}\right)\right)G_R\left(e^{j\left(\omega+n\frac{2\pi}{T_s}\right)T_f}\right)H_{T_s/T_f}\left(e^{j\left(\omega+n\frac{2\pi}{T_s}\right)T_f}\right)U^{T_s}\left(e^{j\left(\omega+n\frac{2\pi}{T_s}\right)NT_f}\right) \tag{27}$$

This expression allows further simplification since

$$H_{T_f}\left(j\left(\omega+n\frac{2\pi}{T_s}\right)\right)H_{T_s/T_f}\left(e^{j\left(\omega+n\frac{2\pi}{T_s}\right)T_f}\right)=\frac{1-e^{-j\left(\omega+n\frac{2\pi}{T_s}\right)T_f}}{j\left(\omega+n\frac{2\pi}{T_s}\right)}\cdot\frac{1-e^{-j\left(\omega+n\frac{2\pi}{T_s}\right)NT_f}}{1-e^{-j\left(\omega+n\frac{2\pi}{T_s}\right)T_f}}=\frac{1-e^{-j\omega T_s}}{j\left(\omega+n\frac{2\pi}{T_s}\right)}=H_{T_s}\left(j\left(\omega+n\frac{2\pi}{T_s}\right)\right) \tag{28}$$

and thus

$$Y^{T_s}(e^{j\omega T_s})=\left(\frac{1}{T_s}\sum_{n=-\infty}^{\infty}P\left(j\left(\omega+n\frac{2\pi}{T_s}\right)\right)G_R\left(e^{j(\omega+n\frac{2\pi}{T_s})T_f}\right)H_{T_s}\left(j\left(\omega+n\frac{2\pi}{T_s}\right)\right)\right)U^{T_s}(e^{j\omega T_s}) \tag{29}$$

Now, the expression between parenthesis is exactly $P_L\left(e^{j\omega T_s}\right)$, that is

$$Y^{T_s}\left(e^{j\omega T_s}\right)=P_L\left(e^{j\omega T_s}\right)\cdot U^{T_s}\left(e^{j\omega T_s}\right) \tag{30}$$

Finally, taking into account that $U^{T_s}\left(e^{j\omega T_s}\right)=G_L\left(e^{j\omega T_s}\right)\left(F_L\left(e^{j\omega T_s}\right)R^{T_s}\left(e^{j\omega T_s}\right)-Y^{T_s}\left(e^{j\omega T_s}\right)\right)$, substituting in (30), and reordering to obtain $Y^{T_s}\left(e^{j\omega T_s}\right)$, the desired result (18) is directly obtained from:

$$Y^{T_s}\left(e^{j\omega T_s}\right)=\frac{G_L\left(e^{j\omega T_s}\right)P_L\left(e^{j\omega T_s}\right)}{1+G_L\left(e^{j\omega T_s}\right)P_L\left(e^{j\omega T_s}\right)}F_L\left(e^{j\omega T_s}\right)\cdot R^{T_s}\left(e^{j\omega T_s}\right) \tag{31}$$

In addition, from (4) and (31) the error spectrum $E^{Ts}\left(e^{j\omega T_s}\right)$ is directly given by

$$E^{T_s}\left(e^{j\omega T_s}\right)=F_L\left(e^{j\omega T_s}\right)R^{T_s}\left(e^{j\omega T_s}\right)-Y^{T_s}\left(e^{j\omega T_s}\right)=S_L\left(e^{j\omega T_s}\right)F_L\left(e^{j\omega T_s}\right)R^{T_s}\left(e^{j\omega T_s}\right) \tag{32}$$

Moreover, since $Y(j\omega)=P(j\omega)U(j\omega)$ then the spectrum of the continuous-time signal y is given by

$$Y(j\omega)=P(j\omega)H_{T_f}(j\omega)G_R\left(e^{j\omega T_f}\right)H_{T_s/T_f}\left(e^{j\omega T_f}\right)G_L\left(e^{j\omega T_s}\right)E^{T_s}\left(e^{j\omega T_s}\right) \tag{33}$$

where, using (26), (28) (for $n=0$), and (32), the desired result (17) is directly obtained. ■

Remark 2. To compute the closed-loop response of the DR control system of Figure 1 to a harmonic reference input with frequency ω_0, that is $r(t)=e^{j\omega_0 t}$, $t\in(-\infty,\infty)$ and

$$R^{T_s}\left(e^{j\omega T_s}\right)=\frac{2\pi}{T_s}\sum_{k=-\infty}^{k=\infty}\delta\left(\omega-\omega_0-k\frac{2\pi}{T_s}\right) \tag{34}$$

Equation (17) can be directly used. The result is a multiharmonic response as expected, given by

$$Y(j\omega)=\frac{2\pi}{T_s}F_L(e^{j\omega_0 T_s})\sum_{k=-\infty}^{k=\infty}T\left(j\omega_0+k\frac{2\pi}{T_s}\right)\delta\left(\omega-\omega_0-k\frac{2\pi}{T_s}\right) \tag{35}$$

from which it is directly obtained the time response

$$y(t) = F_L(e^{j\omega_0 T_s}) \sum_{k=-\infty}^{k=\infty} T\left(j\omega_0 + k\frac{2\pi}{T_s}\right) e^{j\left(\omega_0 + k\frac{2\pi}{T_s}\right)t} \tag{36}$$

Moreover, if the reference is $r(t) = \cos(\omega_0 t)$, considering the symmetry property $T(-j\omega) = T^*(j\omega)$, it easily follows that the time response is

$$y(t) = F_L(e^{j\omega_0 T_s})\left(|T(\omega_0)|\cos(\omega_0 t + \angle T(j\omega_0) + \sum_{k=1}^{k=\infty} |T_k(j\omega_0)|\cos(\omega_k t + \angle T_k(j\omega_0) + |T_k(-j\omega_0)|\cos(-\omega_k t + \angle T_k(-j\omega_0)\right) \tag{37}$$

consisting of the fundamental frequency ω_0 and a infinite number of harmonics at frequencies $\pm\omega_k = \pm\omega_0 + k\frac{2\pi}{T_s}$, $k = 1, 2, 3, \ldots$. Note that the exact time response can be computed by reading the Bode plot of the complementary sensitivity function $T(j\omega)$ at the frequencies given by the fundamental frequency and the harmonics frequencies.

Example 2. Consider the example of Section 3.1. Figure 6 shows the Bode plot of $T(j\omega)$, that has been computed using (16). Here, the time closed-loop response to a reference $r(t) = \cos\left(\frac{\pi}{0.4}t\right)$ can be obtained for a given prefilter, using (37), by computing the magnitude and angle of $T(j\omega)$ for frequencies $\frac{\pi}{0.4}$, $\frac{\pi}{0.4} + k\frac{2\pi}{0.4} = \frac{(2k+1)\pi}{0.4}$, and $-\frac{\pi}{0.4} + k\frac{2\pi}{0.4} = \frac{(2k-1)\pi}{0.4}$, for $k = 1, 2, \ldots$. Thus, the frequencies appearing at the output y are:

$$\frac{\pi}{0.4}, \frac{3\pi}{0.4}, \frac{5\pi}{0.4}, \cdots, \frac{\pi}{0.4}, \frac{3\pi}{0.4}, \frac{5\pi}{0.4}, \cdots \tag{38}$$

Note that only for the first two frequencies $\frac{\pi}{0.4}$, $\frac{3\pi}{0.4}$, the magnitude Bode plot has significant values (for the rest of frequencies the magnitude is under −40 dB). These frequencies are the input frequency $\frac{\pi}{T_s}$ and the frequency $\frac{3\pi}{T_s}$ in which the ripple is produced. For the case $F_L(e^{j\omega_0 T_s}) = 1$, applying (37) the result is well approximated by

$$y(t) \approx 2\left|T\left(j\frac{\pi}{0.4}\right)\right|\cos\left(\frac{\pi}{0.4}t + \angle T\left(j\frac{\pi}{0.4}\right)\right) + 2\left|T\left(j\frac{3\pi}{0.4}\right)\right|\cos\left(\frac{3\pi}{0.4}t + \angle T\left(j\frac{(3)\pi}{0.4}\right)\right) \tag{39}$$

In Figure 6, the values $T\left(j\frac{\pi}{0.4}\right) = 0.2545e^{-j178.5^\circ}$, $T\left(j\frac{3\pi}{0.4}\right) = 0.3166e^{-j265.3^\circ}$, $T\left(j\frac{5\pi}{0.4}\right) = 0.0021e^{-j344.3^\circ}$, $\ldots$, are explicitly marked. A plot of the closed-loop output y as given by (39) is given in Figure 7, where in addition it is shown the time response simulation of the DR control system (note that $r^{T_s}(n) = e^{j\pi n}$, for $n \geq 0$). The response given by (39) is a very good approximation of the steady-state simulated response (a exact value would be obtained by considering the infinite number of harmonics).

For a unit step reference the spectra are $R(j\omega) = \frac{1}{j\omega} + \pi\delta(\omega)$ and $R^{T_s}\left(e^{j\omega T_s}\right) = \frac{1}{1-e^{-j\omega T_s}} + \frac{\pi}{T_s}\sum_{k=-\infty}^{\infty}\delta\left(\omega - k\frac{2\pi}{T_s}\right)$. Now, consider a first order prefilter with $F(s) = \frac{1}{0.1s+1}$ and $F_L(z_s) = \frac{1-e^{-10T_s}}{z_s - e^{-10T_s}}$. The spectrum of the step response is now (note that $F_L(e^{j\omega T_s}) = 1$ for $\omega = k\frac{2\pi}{T_s}$ and any integer k)

$$Y(\omega) = T(j\omega)F_L\left(e^{j\omega T_s}\right).\frac{1}{1-e^{-j\omega T_s}} + \frac{\pi}{T_s}\sum_{k=-\infty}^{\infty} T\left(jk\frac{2\pi}{T_s}\right)\delta\left(\omega - k\frac{2\pi}{T_s}\right) \tag{40}$$

which has a significant component $\left|Y\left(\frac{3\pi}{0.4}\right)\right| \approx 0.1527$ at the ripple frequency as expected. It turns out that a simple way to avoiding ripples and to obtain a good step tracking over the continuous-time domain is to limit the value of $|T(j\omega)|$ at some design frequencies. More precisely, the continuous-time tracking specification will be related with making small $|E(j\omega)/R(j\omega)|$ over the working frequencies interval (*working* or *design* frequencies refer to the chosen set of frequencies for which design specifications are produced), where from (4) and (17) it is obtained

$$|E(j\omega)/R(j\omega)| = |F(j\omega)| \cdot \left|1 - T(j\omega)\frac{F_L\left(e^{j\omega T_s}\right)}{F(j\omega)}\frac{R^{T_s}\left(e^{j\omega T_s}\right)}{R(j\omega)}\right| \tag{41}$$

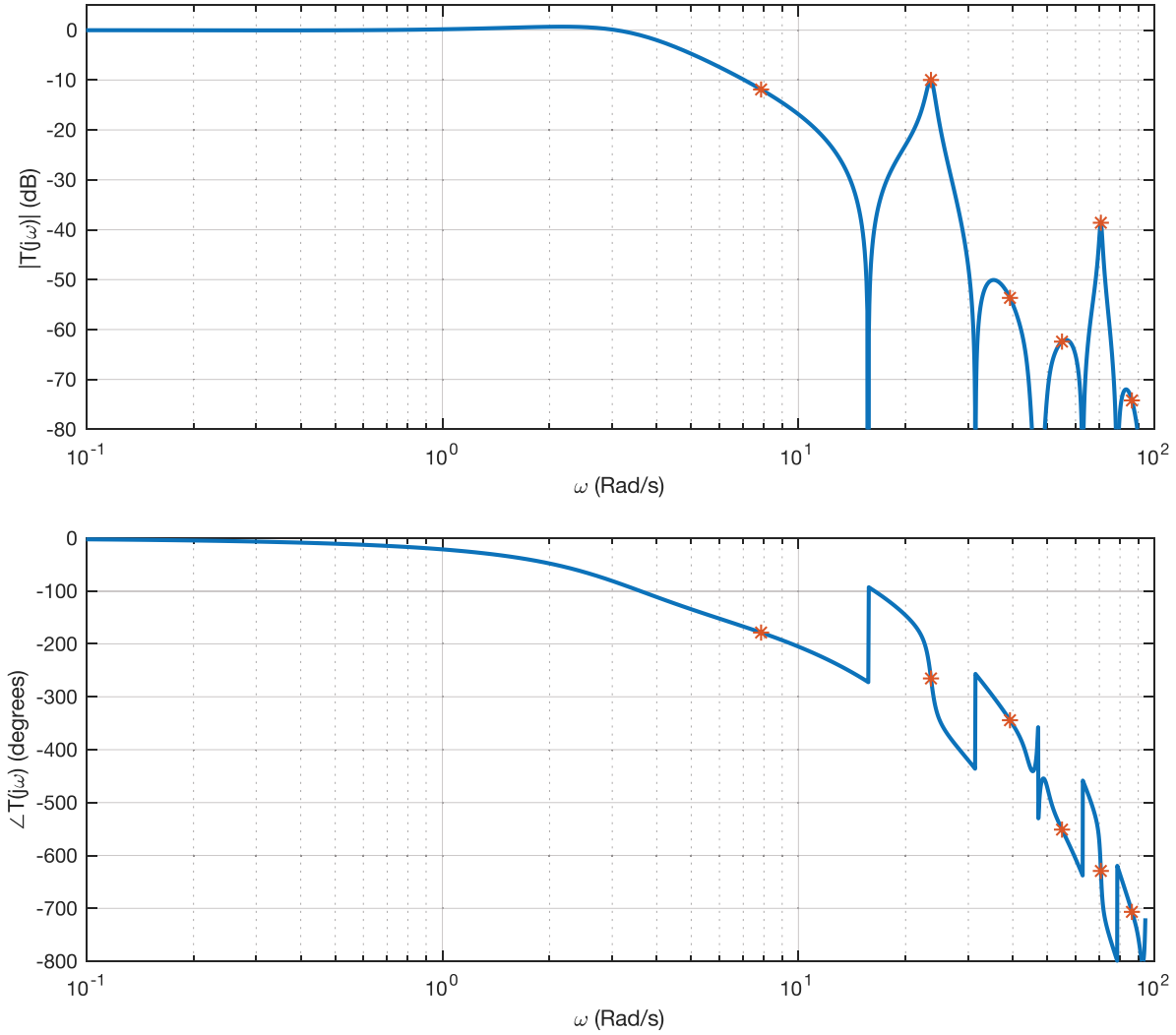

FIGURE 6 Bode plot of the complementary sensitivity function $T(j\omega)$, as given by (16), of Section 3.1 example. This Bode plot contains all the needed information to compute the continuous-time response to a reference input; and, in particular the multifrequency response to a sinusoidal input. The asterisks show the values needed to compute the response to a sinusoidal input of frequency $\frac{\pi}{T_s} \approx 7.85$ Rad/s (in theory, an infinite number of frequencies are needed, but in practice it is enough with the first two frequencies to obtain a good estimate—see Example 2)

This will be the approach to be developed in Section 4, jointly with several other stability and performance design specifications. Note that $E(j\omega)/R(j\omega)$ will be referred to as continuous sensitivity function or simply sensitivity function, and will be denoted by $S(j\omega)$. Note that it is not a sensitivity function or a frequency response in the usual sense, since it depends on the ratio of the continuous-time reference and its sampling. Figure 8 shows the magnitude Bode plot of (41) exhibiting a peak of the sensitivity function of almost 11 dB at the ripple frequency. Clearly, for avoiding the ripple, a specification appropriately limiting the sensitivity function magnitude has to be posed in the control design problem.

4 | MULTIRATE CONTROLLER DESIGN BASED ON QFT

The starting point is a uncertain plant that can be modeled as a set $\mathcal{P}$ of transfer functions. This set may represent physical models with both parametric and non-parametric uncertainty, a set of frequency responses obtained from identifications experiments, and so forth. It is only required that the plant $\mathcal{P}$ be represented by a set of templates $\mathcal{P}_\omega$ that collects all the frequency responses at a frequency $\omega \geq 0$. More specifically, $\mathcal{P}_\omega = \{P(j\omega) : P(s) \in \mathcal{P}\}$. Usually, templates are represented in the Nichols Plane (NC), and it will be assumed that they are simply connected regions of NC and that corresponds to

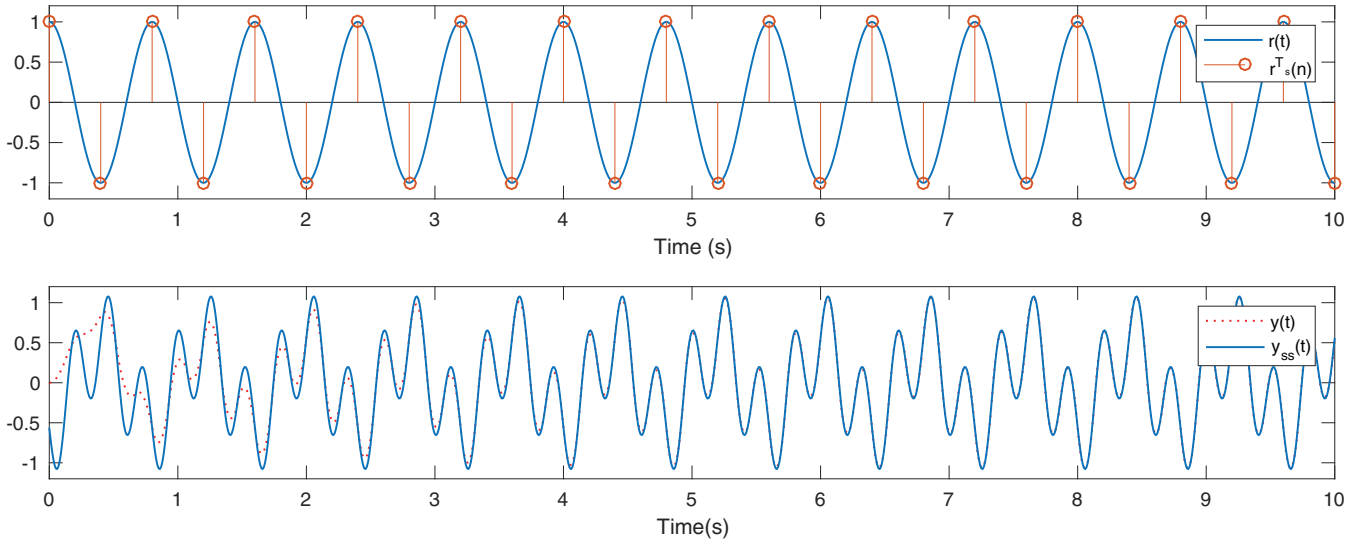

FIGURE 7 (Up) A sinusoidal reference input with frequency $\frac{\pi}{T_s} \approx 7.85$ Rad/s, and its sampling with sampling period $T_s = 0.4$ s; (down) time simulation of the DR control system (dotted), and time response computed using the Bode plot of $T(j\omega)$ (see (39))

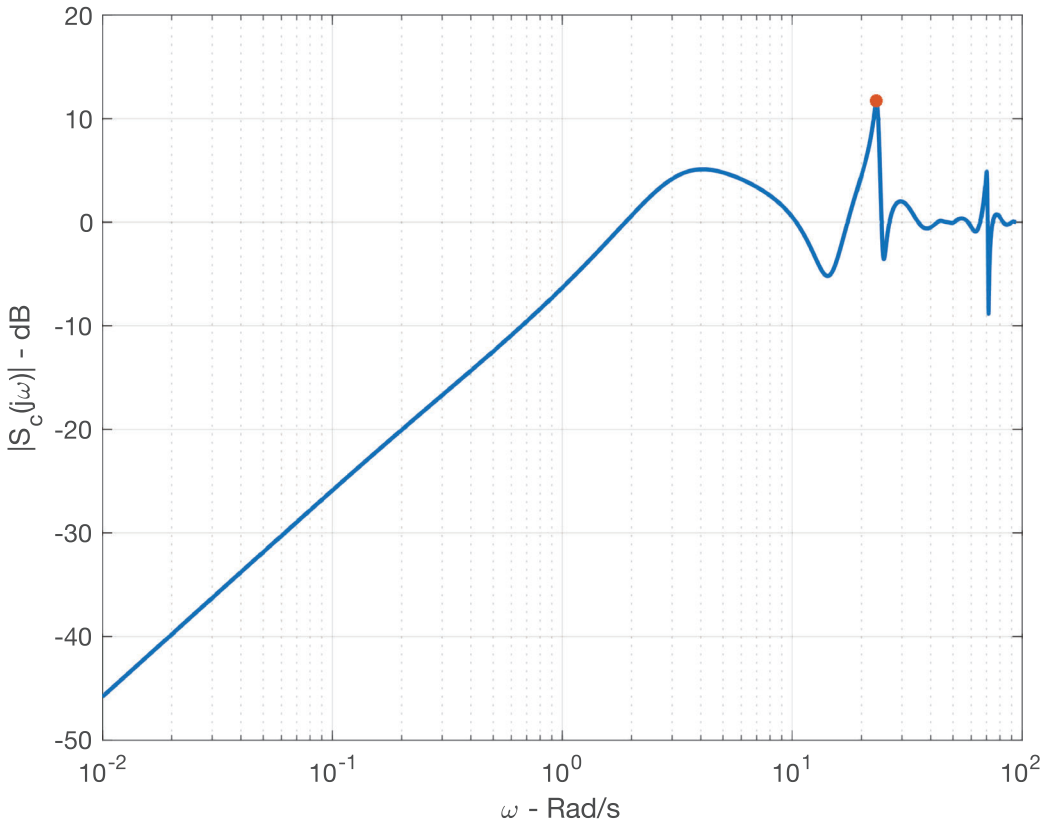

FIGURE 8 Magnitude Bode plot of the continuous sensitivity function for the DR control system of Section 3.1 example (for a unit step reference), see also Example 2. The ripple is clearly exhibited as a peak of approximately 11dB at the frequency $3\pi/T_s$. This sensitivity function is not standard in the sense that it is different for each reference signal, is this case it is related to a step reference

plants with the same number of unstable poles. These restrictions are not overly restrictive and will considerably simplify the design problem, since it will be enough to work with the boundary of the templates.

Now, related with Figure 1, the DR control problem consists of designing the controllers G_R and G_L for an uncertain system $\mathcal{P}$, satisfying design specifications such as stability and tracking for every plant in the set $\mathcal{P}$. More specifically, in this work the design strategy is to design G_L once G_R has been previously design (typically for a nominal plant). The open loop gain function is $L\left(e^{j\omega T_s}\right) = G_L\left(e^{j\omega T_s}\right) P_L\left(e^{j\omega T_s}\right)$, and a nominal value $L_0\left(e^{j\omega T_s}\right) = G_L\left(e^{j\omega T_s}\right) P_{L0}\left(e^{j\omega T_s}\right)$ is obtained for some nominal plant transfer function $P_0 \in \mathcal{P}$. Also, for G_R and a given $P \in \mathcal{P}$ define the discrete uncertainty $\Delta_L\left(e^{j\omega T_s}\right)$ as

$$\Delta_L\left(e^{j\omega T_s}\right) = \frac{P_L\left(e^{j\omega T_s}\right)}{P_{L0}\left(e^{j\omega T_s}\right)} \tag{42}$$

where $P_L = S_N P_R G_R Q_N^*$ and $P_R = S_T P H_T$ (see Section 3.2). In addition, the discrete uncertainty set is defined as $\mathcal{Q}_L = \left\{\Delta_L\left(e^{j\omega T_s}\right) : P \in \mathcal{P}\right\}$. Note that its nominal value is $\Delta_{L0} = 1$. Moreover, the uncertainty $\Delta(j\omega)$ is defined as

$$\Delta(j\omega) = \frac{P(j\omega) G_R\left(e^{j\omega T_f}\right)}{P_{L0}\left(e^{j\omega T_s}\right)} \tag{43}$$

and the uncertainty set as $\mathcal{Q} = \{\Delta(j\omega) : P \in \mathcal{P}\}$.

The QFT design will be based on the loop gain-phase shaping of the nominal loop gain $L_0\left(e^{j\omega T_s}\right)$ for the dual control system to satisfy robust design specifications. In the following, robust stability and tracking specifications are considered.

4.1 | Robust stability

A direct application of Proposition 1 result in that the DR control system is robustly stable, that it is stable for every $P \in \mathcal{P}$, if it is stable for the nominal plant P_0, and in addition for any $\omega \in [0, \pi/T_s]$ and $\Delta_L \in \mathcal{Q}_L$ it is satisfied that

$$1 + L_0\left(e^{j\omega T_s}\right) \Delta_L\left(e^{j\omega T_s}\right) \neq 0. \tag{44}$$

This follows from the fact that all the plants in $\mathcal{P}$ have the same number of unstable poles and thus all the open loop gain functions must cross the ray $\mathbf{R}_0$ the same net number of times. A more restrictive robust stability condition, including stability margins is that for some positive real number $\mu < 1$

$$\left|1 + L_0\left(e^{j\omega T_s}\right) \Delta_L\left(e^{j\omega T_s}\right)\right| \geq \mu \tag{45}$$

for any $\omega \in [0, \pi/T_s]$ and any $\Delta_L \in \mathcal{Q}_L$. Note that this is equivalent for the discrete sensitivity function to satisfy $|S\left(e^{j\omega T_s}\right)| \leq 1/\mu$.

For a given frequency $\omega \in [0, \pi/T_s]$ and any $\Delta_L \in \mathcal{Q}_L$, (45) defines a forbidden region for $L_0\left(e^{j\omega T_s}\right)$ at the frequency ω around the critical point $(-180°, 0\ \text{dB})$ in the Nichols plane, whose boundary will be referred to as stability bound. Note that, in particular, stability bounds guarantees worst-case phase and gain margins as given by $\text{PM} = 180° + 2\cos^{-1}(\mu/2)$ and $\text{GM} = 1/(1-\mu)$, respectively. μ will be referred to as the (worst-case) stability margin.

Example 3. Consider the uncertain plant $\mathcal{P}$ given by

$$\mathcal{P} = \left\{ \frac{a}{(s+0.5)(s+a)} : a \in [0.5, 2.5] \right\} \tag{46}$$

where the nominal plant P_0 corresponds to $a = 1.5$. The question is if the DR controller given by (6)–(7), that has been show to stabilize the DR control system for the nominal case (see Figure 4), is also able to guaranty stability for any plant in the uncertain plant set $\mathcal{P}$. A stability margin $\mu = 0.5$ is chosen, corresponding to $\text{PM} = 28.95°$ and $\text{GM} = 2$.

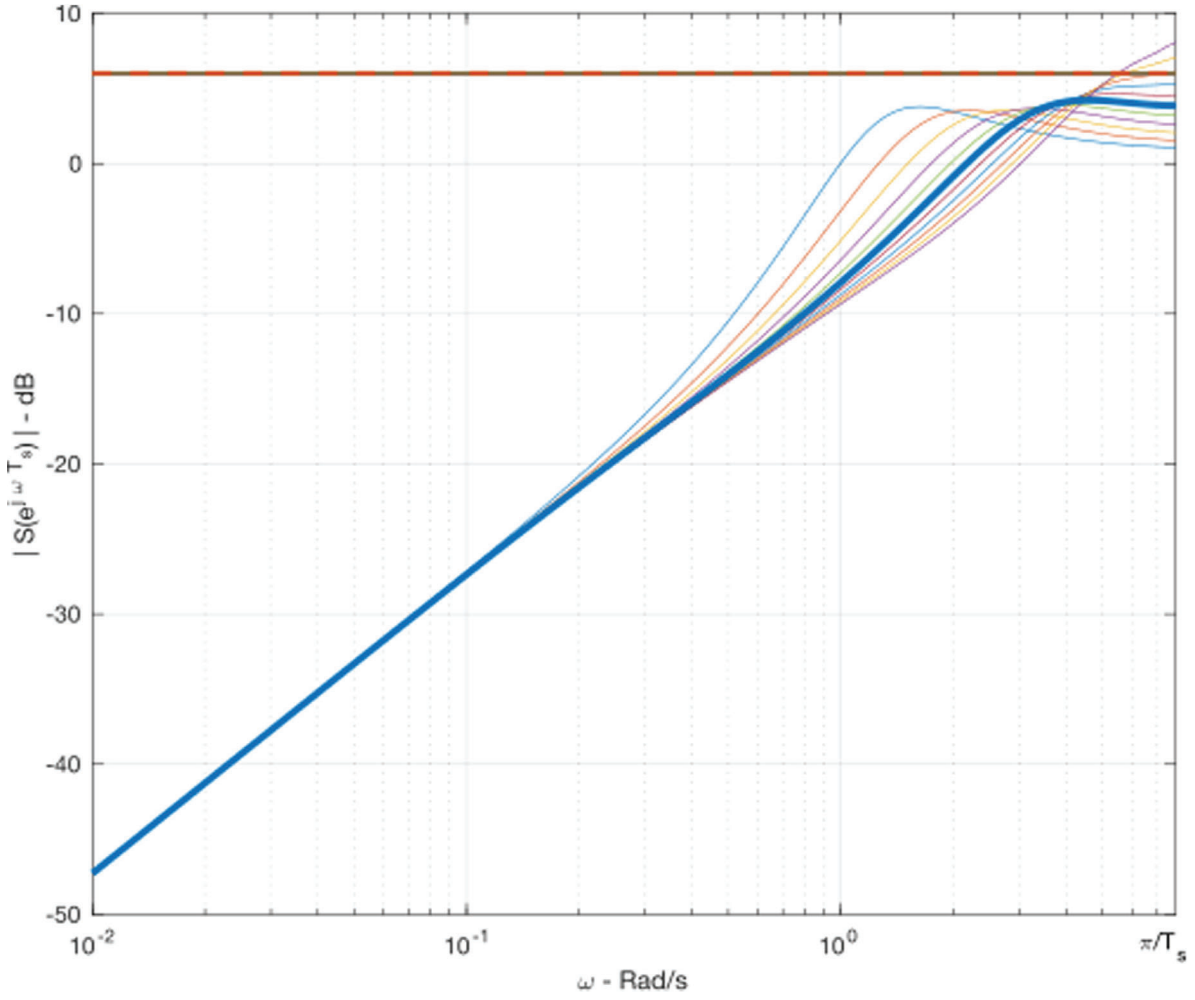

FIGURE 9 Discrete sensitivity magnitude against frequency, for the DR control system of Example 3. The system does not satisfy the worst-case stability margin $\mu = 0.5$ ($1/\mu = 2 \approx 6$ dB) for $a > 2.07$

The analysis will be performed in three (equivalent) ways, for emphasizing the use of stability bounds specially for readers not familiarized with QFT:

- (Discrete sensitivity) It is directly computed $|S\left(e^{j\omega T_s}\right)|$ for $a \in [0.5, 2.5]$. It is not difficult to see that in fact the specification $|S\left(e^{j\omega T_s}\right)| \leq 2$ is not satisfied for high frequencies close to the Nyquist frequency $\frac{\pi}{T_s}$ and $a > 2.07$ (Figure 9). Thus the DR control system is not stable with a stability margin $\mu = 0.5$. Note that it would be stable for $a \in [0.5, 2]$.
- (Open-loop gain functions) Here stability is based on the computation of $L\left(e^{j\omega T_s}\right) = G_L\left(e^{j\omega T_s}\right) P_{L0}\left(e^{j\omega T_s}\right) \Delta_L\left(e^{j\omega T_s}\right)$, for every $\Delta_L \in \mathcal{Q}_L$. Figure 10-left shows the Nichols plots for some values of the parameter a. Note that in this case the stability specification $|1 + L\left(e^{j\omega T_s}\right)| \geq \mu$ results in a forbidden region for any $L\left(e^{j\omega T_s}\right)$ in the Nichols plane (it is bound is shown in Figure 10-left). It is clear that some $L\left(e^{j\omega T_s}\right)$ enter in that forbidden region for some values of the parameter a and thus the DR control system is not stable with the specified stability margin μ.
- (Nominal open-loop gain function) The above stability analysis may be appropriate for analysis but are not well suited for design, since in general it is not obvious how a modification of the controllers (in our case the slow controller G_L) would shape the sensitivity functions or the open-loop gain functions to satisfy the stability specification. A more convenient way both for analysis and design is proposed by using a QFT approach. Basically, the stability specification (45) is translated to a set of forbidden regions of the nominal open-loop gain function $L_0\left(e^{j\omega T_s}\right)$ ideally for every frequency $\omega \in [0, \pi/T_s]$ (in practice, it is enough with a finite number of working frequencies, and some iteration may be needed if the design is not validated). Figure 10-right shows the forbidden regions bounds at several working frequencies. It results that the nominal open-loop function enters the forbidden region for $\omega = \pi/T_s$ and thus the DR control system

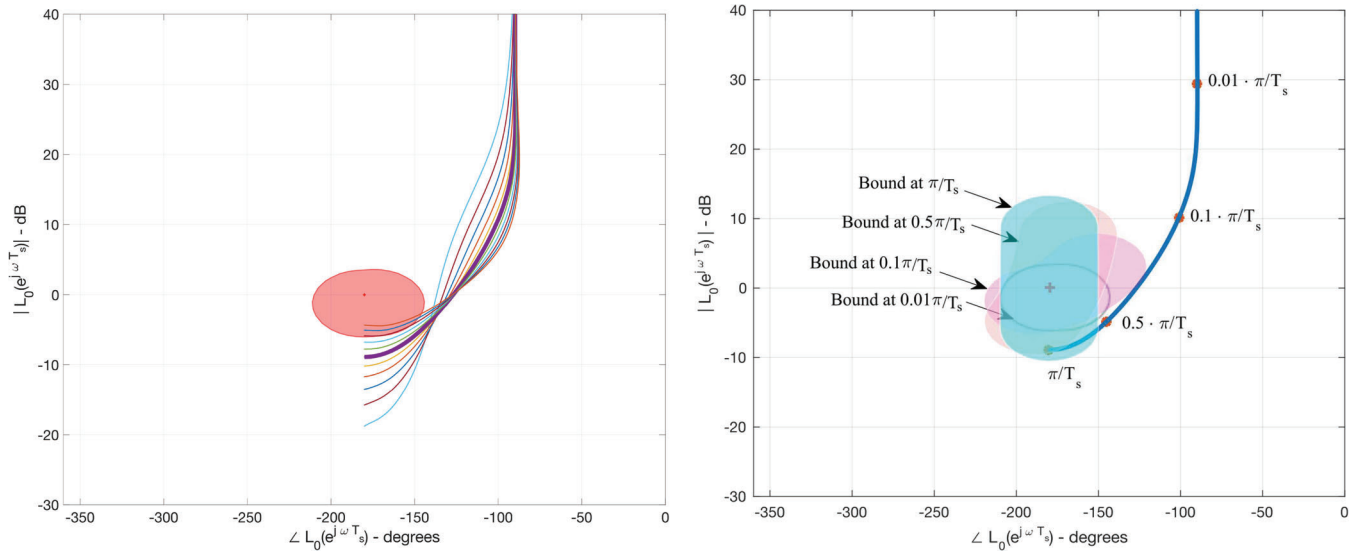

FIGURE 10 (Left) Nichols plots of the open-loop gain functions $L\left(e^{j\omega T_s}\right)$, for some sample values of the parameter $a \in [0.5, 2.5]$ (nominal open loop gain corresponds to $a = 1.5$ -thick line-), and forbidden region in NP for robust stability; (right) Forbidden regions in NP for the nominal open loop gain function, limited by boundaries at several frequencies $\omega \in \{0.01, 0.1, 0.5, 1\} \cdot \pi/T_s$. In both cases, the plots segment from $\omega = 0^-$ to $\omega = 0^+$ (see Figure 5) has not been explicitly shown

violates the robust stability specification. To robustly stabilize the DR control system the nominal open-loop function should be conveniently shaped to be out of the forbidden regions at any frequency.

4.2 | Robust tracking

Reference tracking specifications are considered both in discrete-time and in continuous-time.

Discrete-time tracking

Tracking is specified at the slow sampling period T_s. The transfer function from r^{T_s} to e^{T_s} is $S_L\left(e^{j\omega T_s}\right) F_L\left(e^{j\omega T_s}\right)$, and the discrete-time tracking specification is $\left|E^{T_s}\left(e^{j\omega T_s}\right)/R^{T_s}\left(e^{j\omega T_s}\right)\right| \leq \delta_1(\omega)$ for any reference signal $R^{T_s}\left(e^{j\omega T_s}\right)$, for any $\omega \in [0, \pi/T_s]$ and $P \in \mathcal{P}$. Here $\delta_1 : [0, \pi/T_s] \to \mathbb{R}_{\geq 0}$ is a given function that defines the tracking specification. It easily follows that this is equivalent to

$$\left|1 + L_0\left(e^{j\omega T_s}\right) \Delta_L\left(e^{j\omega T_s}\right)\right| \geq \frac{\left|F_L\left(e^{j\omega T_s}\right)\right|}{\delta_1(\omega)} \tag{47}$$

for any $\omega \in [0, \pi/T_s]$ and $\Delta_L \in \mathcal{Q}_L$. Note that for a given prefilter F_L and a tracking specification δ_1, (47) takes the same form that (45), that is it defines forbidden regions in the NP for the nominal open-loop gain function $L_0\left(e^{j\omega T_s}\right)$, for any $\omega \in [0, \pi/T_s]$.

Continuous-time tracking.

Tracking may be also specified in the continuous-time domain. Here the only limitation is that a tracking specification must be posed for some given reference. This limitation is directly related with the time-varying nature of the DR control system, and it can be alleviated by using as much tracking specifications as needed and using the worst-case. The tracking specification is $|E(j\omega)/R(j\omega)| \leq \delta_2(\omega)$ for a given reference R, any $\omega > 0$, and any $P \in \mathcal{P}$. Note that the specification will result in restrictions over the nominal open-loop function $L_0\left(e^{j\omega T_s}\right)$ for frequencies below and beyond the Nyquist frequency π/T_s, and thus continuous-time tracking specifications for $\omega > \pi/T_s$ will be folded over the interval $[0, \pi/T_s]$.

As a consequence, and to the authors knowledge this is a previously unexplored case in QFT, for the frequencies in which $L_0\left(e^{j\omega T_s}\right)$ can be designed, that is for $\omega \in [0, \pi/T_s]$, in practice there will be a finite number of restrictions or boundaries to be satisfied resulting from the folding of specifications for frequencies beyond π/T_s (note that usually it is enough with continuous-time tracking specifications for frequencies not much larger that the crossover frequency). The following result gives a procedure for obtaining continuous-time tracking bounds; as usual, the worst-case boundary will be used for shaping the nominal open loop gain function.

Proposition 3. *Consider the DR control system of Figure 1, and assume that it is stable and that Assumption 1 holds. For a given frequency $\omega > 0$ and a reference R, the continuous-time tracking specification $|E(j\omega)/R(j\omega)| \leq \delta_2(\omega)$ for any $P \in \mathcal{P}$, is equivalent to the following specification: if $\omega \in \left[k\frac{2\pi}{T_s}, \left(2k+1\right)\frac{\pi}{T_s}\right]$ for some $k = 0, 1, 2, \ldots$ then*

$$\left|\frac{1 + L_0(e^{j\omega^\dagger T_s})A(j\omega)}{1 + L_0(e^{j\omega^\dagger T_s})\Delta_L(e^{j\omega^\dagger T_s})}\right| \leq \frac{\delta_2(\omega)}{|F(j\omega)|} \tag{48}$$

is satisfied by $L_0(e^{j\omega^\dagger T_s})$ at a frequency $\omega^\dagger = \omega - k\frac{2\pi}{T_s} \in [0, \pi/T_s]$ and any $\Delta \in \mathcal{Q}$ and $\Delta_L \in \mathcal{Q}_L$; alternatively, if $\omega \in \left[\left(2k+1\right)\frac{\pi}{T_s}, (k+1)\frac{2\pi}{T_s}\right]$ for some $k = 0, 1, 2, \ldots$, then

$$\left|\frac{1 + L_0^*(e^{j\omega^\dagger T_s})A(j\omega)}{1 + L_0^*(e^{j\omega^\dagger T_s})\Delta_L^*(e^{j\omega^\dagger T_s})}\right| \leq \frac{\delta_2(\omega)}{|F(j\omega)|} \tag{49}$$

is satisfied by $L_0(e^{j\omega^\dagger T_s})$ at a frequency $\omega^\dagger = -\omega + (k+1)\frac{2\pi}{T_s} \in [0, \pi/T_s]$ and any $\Delta \in \mathcal{Q}$ and $\Delta_L \in \mathcal{Q}_L$. In both cases,

$$A(j\omega) = \Delta_L\left(e^{j\omega T_s}\right) - \frac{F_L\left(e^{j\omega T_s}\right) R^{T_s}\left(e^{j\omega T_s}\right)}{F(j\omega)R(j\omega)}\Delta(j\omega) \tag{50}$$

Proof. Using (4), (15)–(17), $E(j\omega)/R(j\omega)$ is given by

$$\frac{E(j\omega)}{R(j\omega)} = F(j\omega) - \frac{Y(j\omega)}{R(j\omega)} = F(j\omega) - \frac{P(j\omega)G_R(e^{j\omega T_f})H_{T_s}(j\omega)G_L\left(e^{j\omega T_s}\right)}{1 + P_L\left(e^{j\omega T_s}\right)G_L\left(e^{j\omega T_s}\right)}F_L\left(e^{j\omega T_s}\right)\frac{R_L\left(e^{j\omega T_s}\right)}{R(j\omega)} \tag{51}$$

Moreover, from (42) and (43), (51) is equal to

$$\frac{E(j\omega)}{R(j\omega)} = F(j\omega) - \frac{\Delta(j\omega)L_0\left(e^{j\omega T_s}\right)}{1 + \Delta_L\left(e^{j\omega T_s}\right)L_0\left(e^{j\omega T_s}\right)}F_L\left(e^{j\omega T_s}\right)\frac{R_L\left(e^{j\omega T_s}\right)}{R(j\omega)} \tag{52}$$

Now, to obtain (48), $E(j\omega)/R(j\omega)$ must be expressed in the form

$$\frac{E(j\omega)}{R(j\omega)} = \frac{1 + L_0\left(e^{j\omega T_s}\right)A(j\omega)}{1 + L_0\left(e^{j\omega T_s}\right)\Delta_L\left(e^{j\omega T_s}\right)}F(j\omega) \tag{53}$$

and thus equalizing the right-hands of (52) and (53) it easily follows that (the frequency arguments are removed by simplicity)

$$(1 + L_0A)F = F(1 + \Delta_L L_0) - HG_LF_L\frac{R_L}{R} = \left(1 + \Delta_L L_0 - \Delta L_0\frac{F_L R_L}{FR}\right)F \tag{54}$$

and (50) directly follows. Note that is has been proved that the continuous-time tracking specification is equivalent to the nominal open-loop function $L_0\left(e^{j\omega T_s}\right)$ to satisfy the inequality

$$\left|\frac{1 + L_0\left(e^{j\omega T_s}\right)A(j\omega)}{1 + L_0\left(e^{j\omega T_s}\right)\Delta_L\left(e^{j\omega T_s}\right)}\right| \leq \frac{\delta_2(\omega)}{|F(j\omega)|} \tag{55}$$

for any $\omega \geq 0$, any $\Delta_L \in \mathcal{Q}_L$, and any $\Delta \in \mathcal{Q}$.

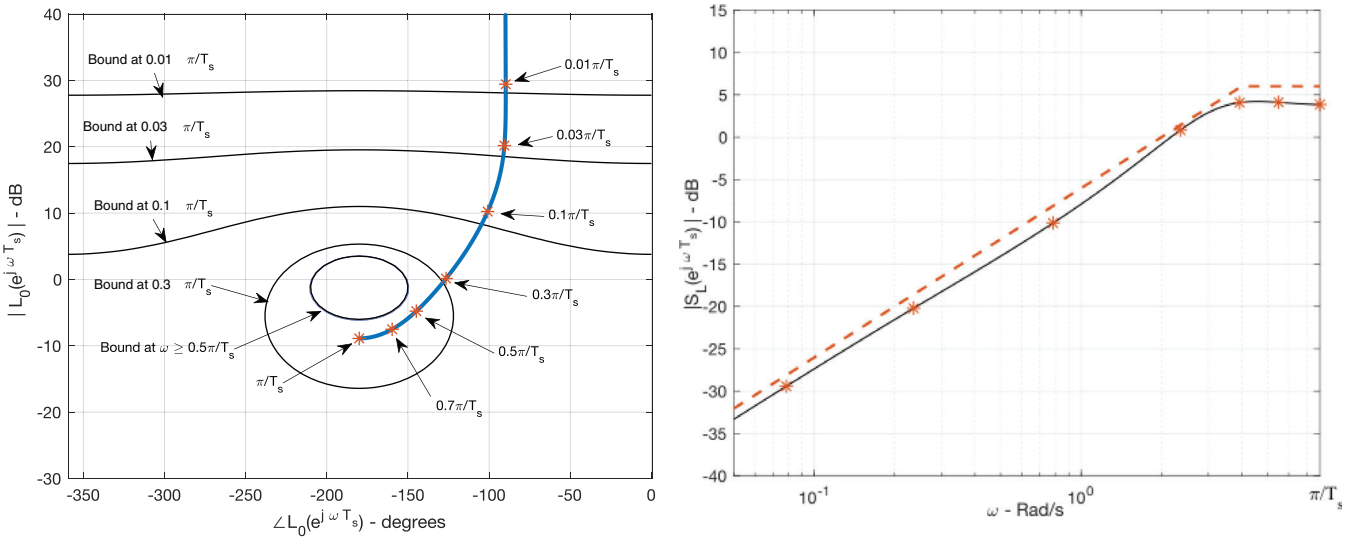

FIGURE 11 (Left) Discrete-time tracking boundaries at the design frequencies set $\{0.01, 0.03, 0.1, 0.3, 0.5, 0.7, 1\} \cdot \pi/T_s$, and nominal open loop gain function $L\left(e^{j\omega T_s}\right)$ -asterisks denote its value at the design frequencies-. (Right) Discrete-time tracking specification as upper bound over $|S_L\left(e^{j\omega T_s}\right)|$ (dotted line), and magnitude Bode plot (solid line) of the resulting $S_L\left(e^{j\omega T_s}\right)$ for the DR control system -asterisks also denote its values at the design frequencies-

To end the proof, periodicity and symmetry properties of $L_0\left(e^{j\omega T_s}\right)$ are recalled to obtain the folding frequency $\omega^\dagger \in [0, \pi/T_s]$ at which the inequality poses a restriction over the nominal open-loop function. If $\omega \in \left[k\frac{2\pi}{T_s}, \left(2k+1\right)\frac{\pi}{T_s}\right]$ for some $k = 0, 1, 2, \ldots$ then at the frequency $\omega^\dagger = \omega - k\frac{2\pi}{T_s} \in \left[0, \frac{\pi}{T_s}\right]$, periodicity of nominal open-loop gain function results in that $L_0\left(e^{j\omega T_s}\right) = L\left(e^{j\left(\omega^\dagger + k\frac{2\pi}{T_s}\right)T_s}\right) = L_0\left(e^{j\omega^\dagger T_s}\right)$. Alternatively, if $\omega \in \left[(2k+1)\frac{\pi}{T_s}, (k+1)\frac{2\pi}{T_s}\right]$ for some $k = 0, 1, 2, \ldots$, then at the frequency $\omega^\dagger = -\omega + (k+1)\frac{2\pi}{T_s} \in \left[0, \frac{\pi}{T_s}\right]$, using symmetry and periodicity arguments it directly follows that $L_0\left(e^{j\omega T_s}\right) = L_0\left(e^{j\left(-\omega^\dagger + (k+1)\frac{2\pi}{T_s}\right)T_s}\right) = L_0\left(e^{-j\omega^\dagger T_s}\right) = L_0^*(e^{j\omega^\dagger T_s})$. The same property holds for $\Delta_L\left(e^{j\omega T_s}\right)$. Considering the inequality (55) in both cases directly gives (48) and (49), respectively. ∎

Example 4. The example of Section 3.1 is now analyzed by using discrete-time and continuous-time tracking specifications using the above QFT specifications. By simplicity, first it is considered the case of no-uncertainty, that is the plant is given by (5). And the slow and fast controllers are given by (6) and (7), respectively. Also, the prefilter is $F(s) = \frac{1}{0.1s+1}$ and it is discretization is $F_L(z_s) = \frac{1-e^{-10T_s}}{z_s - e^{-10T_s}}$.

First, consider a discrete-time tracking specification like (47), that combined with a stability specification like (45), gives a restriction over the discrete-time sensitivity function like $|S_L\left(e^{j\omega T_s}\right)| \leq \min\{\delta_1(\omega)/|F_L\left(e^{j\omega T_s}\right)|, 1/\mu\}$, where $\delta_1(\omega) = \omega/2$ and $\mu = 0.5$ has been chosen. Moreover, the design frequencies $\{0.01, 0.03, 0.1, 0.3, 0.5, 0.7, 1\} \cdot \pi/T_s$ are chosen (note that for the discrete-time sensitivity function the Nyquist frequency π/T_s is the highest frequency). In Figure 11-left both QFT bounds and the open-loop gain function L_0 are plotted. It is clear that the tracking (and stability) specification is satisfied at the working frequencies. However, the design must be validated for the rest of frequencies, this is shown in the 11-right where the design is validated for the discrete-time tracking specification (as it is expected from the results of Section 3.1).

Now, continuous-time tracking specifications are considered, including frequencies below and beyond the Nyquist frequency π/T_s. The continuous-time step tracking specification is $|E(j\omega)/R(j\omega)| \leq \min\{\delta_2(\omega)/|F(j\omega)|, \mu\}$. where $\delta_2(\omega) = \omega/2$ and $\mu = 0.5$. Two sets of frequencies are separately considered in the following.

First, frequencies below the Nyquist frequency; in this case, the same frequencies that the previously used for discrete-time step tracking are used, that is $\{0.01, 0.03, 0.1, 0.3, 0.5, 0.7, 1\} \cdot \pi/T_s$. The resulting boundaries (according to Proposition 3) are shown in Figure 12-left; note that the nominal open loop gain satisfies the restrictions posed by the boundaries, except for the frequency $\omega_4 = 0.3\pi/T_s$ where it slightly crosses the boundary. Figure 12-right shows a Bode plot of the continuous sensitivity magnitude over the frequency interval $[0, \pi/T_s]$, validating the design except for the interval $[0.2, 0.5] \cdot \pi/T_s$ where it slightly crosses the specification bound. In practice, this design is reasonably

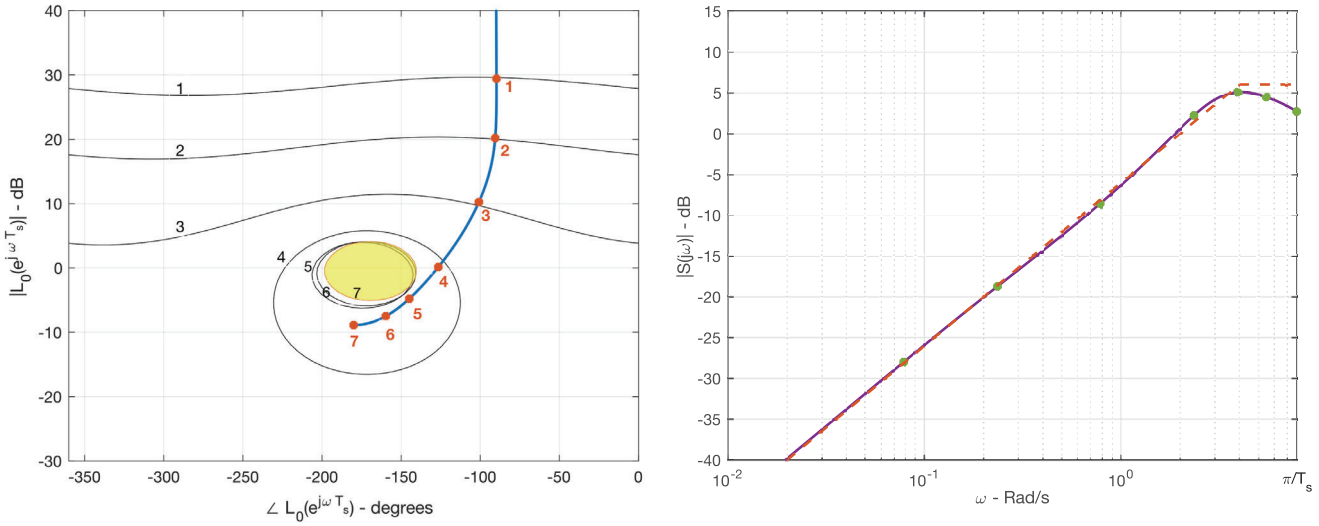

FIGURE 12 Continuous-time tracking for frequencies below the Nyquist frequency π/T_s. (Left) Boundaries at the working frequencies $\omega_{1,2,3,4,5,6,7} = (0.01, 0.02, 0.1, 0.3, 0.5, 0.7, 1) \cdot \pi/T_s$, indexed by the labels $1, 2, \ldots, 7$, and nominal open loop gain $L_0\left(e^{j\omega T_s}\right)$ (thick line) with asterisks denoting its values at the corresponding working frequencies. Open boundaries (#1, #2, #3, with solid line) define a forbidden region below, and close boundaries (#4..#7) define a forbidden region inside. (Right) Magnitude Bode plot of the sensitivity function $S(j\omega)$ (solid line), and specification bound (dotted line)

good and it may be concluded that the DR design, that correctly performs according to discrete-time tracking specifications (see Figure 11), also will satisfactorily track steps as far as frequencies below the slow Nyquist frequency is concerned.

Second, frequencies beyond the Nyquist frequency. The set $\{2.5, 2.75, 3, 3.8, 5, 8.9\} \cdot \pi/T_s$ (note that $3\pi/T_s$ is the ripple frequency. see Figure 8) has been chosen. By using Proposition 3, boundaries are obtained at the folded frequencies $\{0.5, 0.75, 1, 0.2, 1, 0.9\} \cdot \pi/T_s$, see Figure 13-left. Note that in particular there are boundary crossings at $\omega_9^\dagger = 0.75\pi/T_s$ and $\omega_{10}^\dagger = \pi/T_s$, these are the responsible for the ripple in the step response. Figure 13-right is a magnitude Bode plot of the sensitivity function over the interval $[0, 100]$ Rad/s. As a conclusion, the DR design is not validated for frequencies beyond the (slow) Nyquist frequency.

Remark 3. It is worthwhile to emphasize that when analyzing or designing DR controllers for satisfying continuous-time tracking specifications, like in Example 4, the shaping of the (nominal) open-loop gain at every working frequency in $[0, \pi/T_s]$ is the design element, however a particular value a some frequency in that interval is responsible for the shaping of the continuous sensitivity function not only at that same frequency, but also in (infinitely) many frequencies beyond π/T_s. In Example 4, this is reflected for example by the fact that $L(e^{j\pi/T_s})$ (the high-frequency value of the open-loop gain) is constrained by continuous tracking specifications at several frequencies, significatively at π/T_s, $3\pi/Ts$ (the ripple frequency), and $5\pi/Ts$ (also less importantly at higher frequencies $7\pi/Ts$, $9\pi/Ts$, $\ldots$). These constraints are exactly boundaries #7, #10, and #12 (Figures 12 and 13). As a direct consequence, for ripple avoiding the open-loop gain should be redesigned at π/T_s to satisfy the worst-case boundary, which in this case reduces to boundary #10 (Figure 13).

Example 5. In this example, the DR control system of Section 3.1 example is redesigned to avoid the ripple in the step response. According to Example 4 (see also Remark 3), the design action will consists of redesigning the slow controller by reshaping the open-loop gain, to satisfy the constraint posed by boundary #10, obviously without significatively altering it at the rest of frequencies. Looking at Figure 13, the design problem is about to shape the open-loop gain close to the Nyquist frequency to be below the boundary #10. A simple solution is to add a notch filter to the slow controller. The following filter has been used, with design parameters K, α_1, and α_2:

$$N(z) = K\frac{(z-\alpha_1)(z+\alpha_2)}{(z-0.5)(z+0.5)} \tag{56}$$

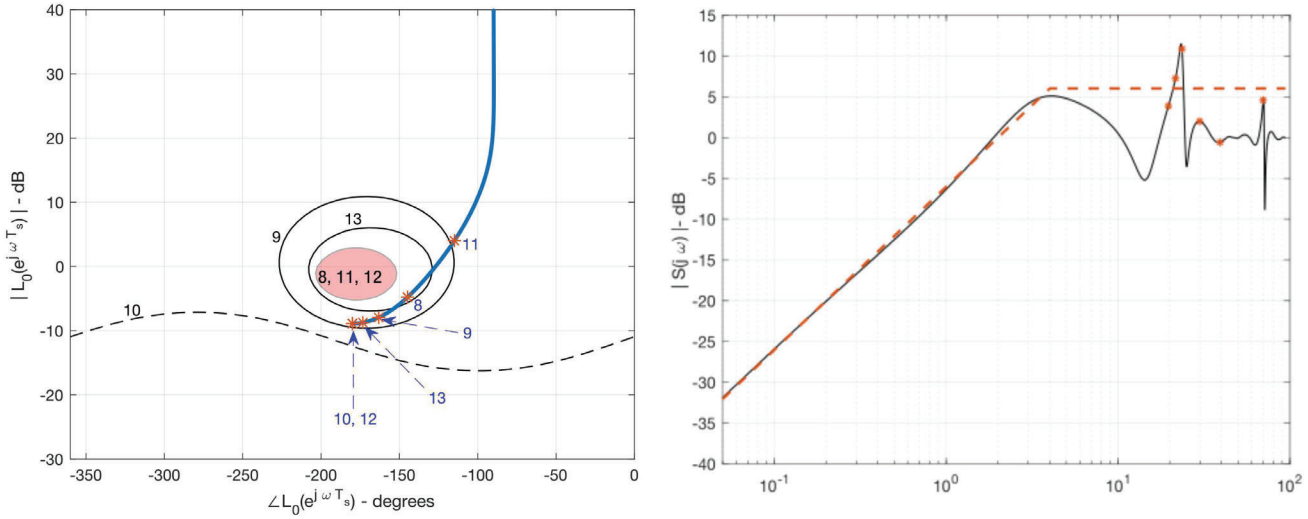

FIGURE 13 Continuous-time tracking for frequencies beyond π/T_s. (Left) Specifications at the working frequencies $\omega_{8,9,10,11,12,13} = (2.5, 2.75, 3, 3.8, 5, 8.9) \cdot \pi/T_s$, result in boundaries at the folded frequencies $\omega^{\dagger}_{8,9,10,11,12,13} = \{0.5, 0.75, 1, 0.2, 1, 0.9\} \cdot \pi/T_s$. The open boundary #10 (dotted line) define the forbidden region above. (Right) Magnitude Bode plot of the sensitivity function $S(j\omega)$ (solid line), and specification bound (dotted line)

After some trial and error, a good solution has been found (the previous design has not been significatively changed at low frequencies), resulting in $\alpha_1 = 0.52$, $\alpha_1 = 0.76$, and $K = 0.75$. Note that the dc-gain of the notch filter is 0.85, which means that the open-loop gain has been detuned at low frequencies to allow it to satisfy restrictions posed by the boundaries at frequencies beyond the Nyquist frequency, including the ripple frequency. Figure 14-left shows the Nichols plot of the open-loop gain including the notch filter, that is $L_0\left(e^{j\omega T_s}\right) = N\left(e^{j\omega T_s}\right) G_L\left(e^{j\omega T_s}\right) P_{L0}\left(e^{j\omega T_s}\right)$. Note that although at low frequencies the open-loop gain has been slightly detuned, there is no much significative differences with the design of Figure 12; however, at frequencies close to the Nyquist frequency π/T_s the open-loop gain satisfies the restrictions posed by boundaries, in particular the boundary #10 which is the dominant boundary corresponding to the ripple frequency. The validation of the design is performed by checking the value of the continuous sensitivity $S(j\omega)$ for frequencies up to $\omega = 100$ Rad/s. In contrast to Figure 13-right, it is shown in Figure 14-right how $S(j\omega)$ clearly satisfies tracking specification for frequencies beyond π/T_s. As it is above discussed, the detuning of the open-loop gain at low frequencies is also clearly seen when comparing both Figures, but it is not considered relevant in practice. Of course, a better design without the need of detuning could be performed but at the cost of using a slow controller with a much higher order. Finally, a time simulation of the initial DR control system and its redesign to avoid the ripple is shown in Figure 15.

5 | APPLICATION

In this section, the QFT design procedure developed above is going to be applied to an unstable system with parametric uncertainty: a reaction wheel balancing. In contrast to Examples 3–5, where besides robust stability the focus was in the performance at frequencies beyond the (slow) Nyquist frequency, in this application case the design challenge will be at low frequencies, below the Nyquist frequency, with the added difficulty posed by the fact that the open-loop system is unstable.

The inverted pendulum is a classical control problem, frequently used as a test-bed to evaluate different control strategies. Among several versions of the inverted pendulum, in the reaction wheel inverted pendulum (RWIP) the motor is located at the top of the pendulum instead than at its base. A flywheel connected to the motor axis generates the torque that keeps the pendulum in its unstable equilibrium position, cancelling the unavoidable disturbances and following a desired reference. Figure 16 shows a CAD model of the RWIP.

An angular position sensor is located at the joint between the pendulum and the base. This sensor is used to measure the angular position of the pendulum, $\theta(t)$.

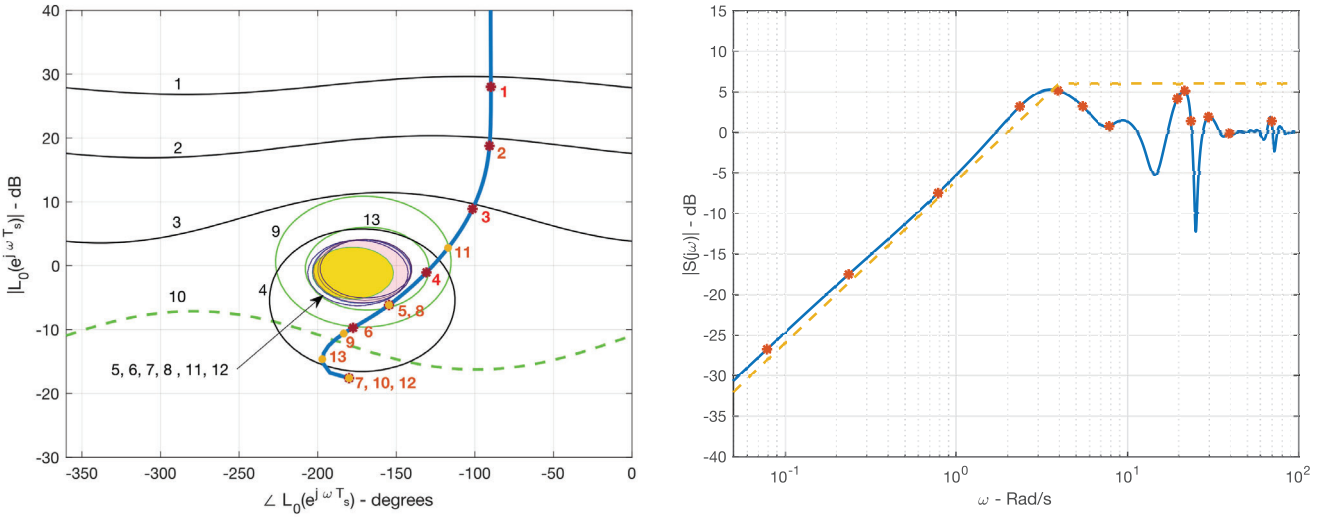

FIGURE 14 Continuous-time tracking for frequencies below and beyond the Nyquist frequency π/T_s. Redesign by using a notch filter. (Left) Boundaries at the working frequencies $\omega_{1,2,\dots,13} = (0.01, 0.02, 0.1, 0.3, 0.5, 0.7, 1, 2.5, 2.75, 3, 3.8, 5, 8.9) \cdot \pi/T_s$, indexed by the labels $1, 2, \dots, 13$, and nominal open loop gain $L_0\left(e^{j\omega T_s}\right)$ over $[0, \pi/T_s]$ (thick line) with asterisks denoting its values at the corresponding working frequencies (note that working frequencies beyond π/T_s are folded). (Right) Magnitude Bode plot of the sensitivity function $S(j\omega)$ (solid line), and specification bound (dotted line)

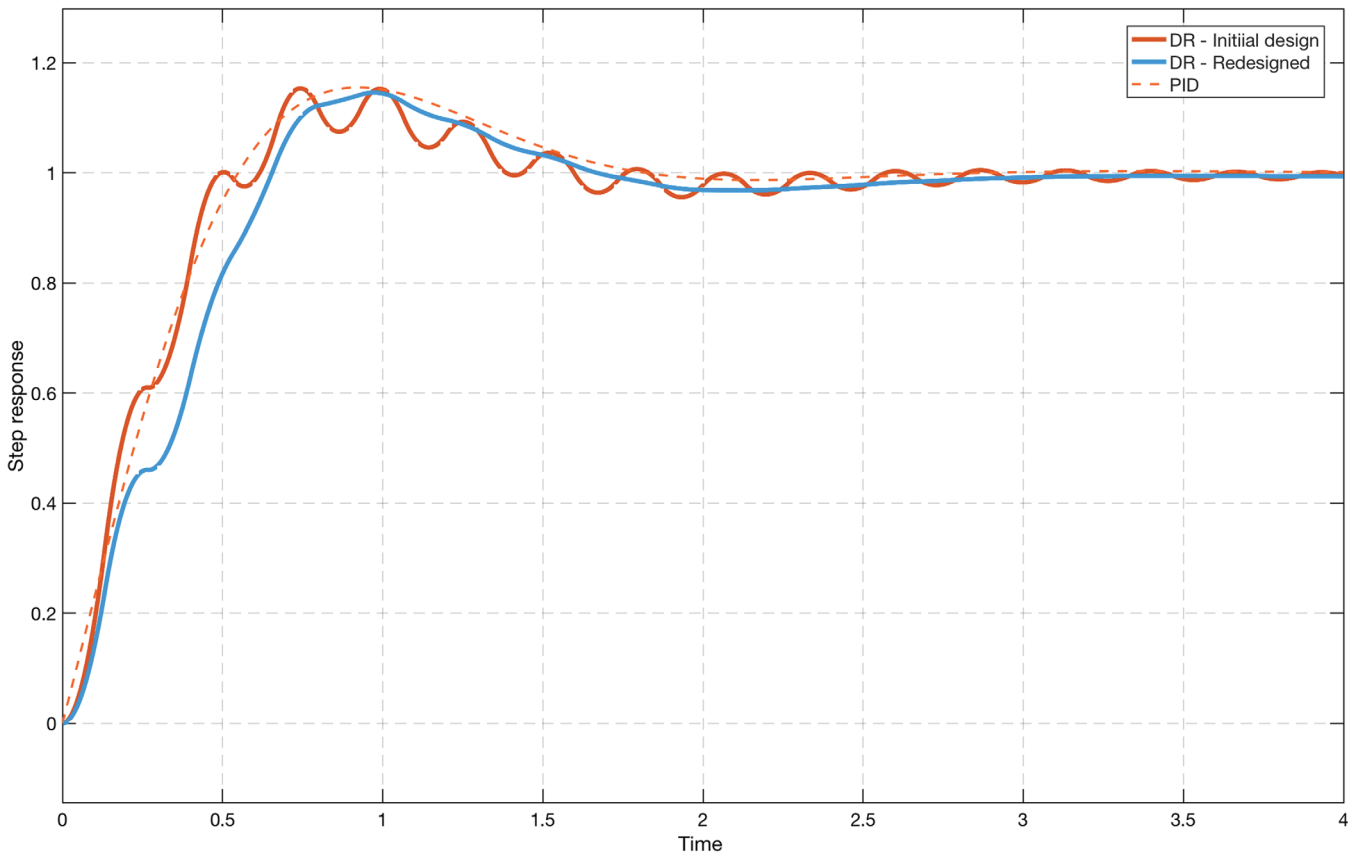

FIGURE 15 Step response of the initial DR control system, the redesigned DR control system, and the corresponding to the PID controller

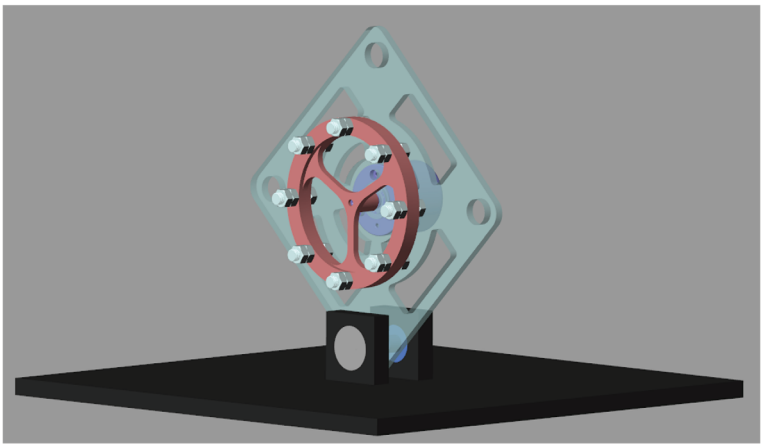

FIGURE 16 Reaction wheel set-up

TABLE 1 Physical constant values for the RWIP

Constant	Value	Units
J_p	413	kg mm^2
m_p	0.233	kg
l_p	84.85	mm
$J_f(nominal)$	290	kg mm^2
m_f	0.147	kg
l_f	84.85	mm
B	0.1	N m/s
g	9.81	m/s^2

A DR control design problem will defined by using stability and tracking specifications, the goal is to move the pendulum following a specified reference, typically a sinusoid. The case of no prefilter, that is, $F(s) = 1$ will be considered. To reach these goals the motor applies a certain torque to the flywheel. The torque causes the angular velocity of the wheel, $w(t)$. The acceleration of the flywheel generate a torsion torque that rotates the pendulum around the joint. In order to design the appropriated controller, a mathematical model of the RWIP is needed. The non-linear equation that describes the relationship between the angular velocity of the flywheel and the angular position of the pendulum is as follows:

$$J_f\dot{w}(t) + \widehat{ML}gsin(\theta(t)) - B\dot{\theta}(t) = J_T\ddot{\theta}(t) \tag{57}$$

being J_T the moment of inertia of the RWIP that can be calculated using the Steiner theorem as follows:

$$J_T = m_p l_p^2 + m_f l_f^2 + J_p + J_f \tag{58}$$

where constants m_p and m_f are the mass of the pendulum (including the motor attached to it) and the flywheel. Constants l_p and l_f are the distance between the rotation point of the pendulum and the center of gravity of pendulum and flywheel (note that in the proposed structured shown in Figure 16 these distances are equal). Constants J_p and J_f are the moments of inertia of the pendulum and flywheel, which depends on its density and geometry. Table 1 shows the values of these parameters, measured in the CAD model of the proposed RWIP.

$\widehat{ML}$ is the product of the masses and distances of the different parts of the RWIP:

$$\widehat{ML} = m_p l_p + m_f l_f \tag{59}$$

Constant B is the viscous friction of the motor joint that must be experimentally determined in the motor that moves the flywheel. Finally, g is the gravitational constant. Nonlinear dynamics from (57) can be easily linearized for small movements around the working point $\theta(t) = 0$, that is, the upwards unstable equilibrium position. The result is the plant transfer function $P(s)$ given by

$$P(s) = \frac{\theta(s)}{w(s)} = \frac{J_f s}{J_T s^2 + Bs - MLg} \tag{60}$$

Moreover, different weights in the flywheel are obtained by allowing a varying number of screws (Figure 16). The nominal value J_f= 290 kg mm^2 may be reduced until a third of it resulting in an uncertain parameter $J_f \in \left[1/3, 1\right]$ 290 kg mm^2 (the correct values of J_f are obtained by means of NX Siemens software). In the following, all the time simulations have been performed using *Simscape Multibody* of Simulink considering all physical constants of our set-up.

The design specifications are robust stability and robust continuous-time tracking: the DR control system must be stable and satisfy some stability margin μ, and also tracks a sinusoidal reference of amplitude 10° and frequency 0.1 Hz; and for any $J_f \in \left[1/3, 1\right]$ 290 kg mm^2. More specifically, a stability margin $\mu = 1/\sqrt{2}$ (corresponding to worst-case margins PM = ≈ 40° and GM ≈ 10 dB) has been chosen. Also, the continuous-time tracking specification is based on a second order model with $\xi = 0.5$ and $\omega_n = 5$, it is given by $\left|\frac{E(j\omega)}{R(j\omega)}\right| \leq \delta_2(\omega)$, where

$$\delta_2(\omega) = \begin{cases} 1 - \frac{5^2}{(j\omega)^2+5(j\omega)+5^2} & \text{if } \omega \leq 5 \; Rad/s \\ \sqrt{2} & \text{if } \omega > 5 \; Rad/s \end{cases} \tag{61}$$

and the reference is the sinusoidal signal $R(j\omega) = A\frac{b}{(j\omega+a)^2+b^2}$ with $A = 10\pi/180$ and $b = 2\pi/10$. Moreover, there are design restrictions regarding the controller digital implementation: the angle measurement should be performed at most each T_s=8 ms, while the control action may be updating with $T_f = 4$ ms.

5.1 | PID-based DR controller

The design procedure starts with a continuous-time PID that has been tuned to satisfy the design specifications for the nominal plant (with $J_f = 290$ kg mm^2). A root-locus based design technique has been used here, but any other tuning method can be used. The result is $G_r(s) = K_r(1 + T_d s + 1/(sT_i))$, with $K_r = 42.2$, $T_d = 0.031$, and $T_i = 3$. Now, this PID is used for a first DR controller design, consisting of a slow (integral) and fast (derivative) parts discretization. In this case, the proportional constant was included in the integral part (although it does not matter to include it in the derivative part). The result (see Reference 55 for computation details) is

$$G_L(z_s) = K_r \frac{z_s - (1 - (t/T_i))}{z_s - 1} = 42.2\frac{z_s - 0.9973}{z_s - 1} \tag{62}$$

$$G_R(z_f) = \frac{(1 + (T_d/T_f))z_f - (T_d/T_f)}{z_f} = \frac{8.817z_f - 0.8866}{z_f} \tag{63}$$

A time simulation of the DR control system with the above controllers is shown in Figure 17, for the nominal case. The result is that the sensitivity function does not satisfy the tracking specification, note that in particular $|E(j0.63)/R(j0.63)| \approx -10$ dB, which is far from the design specification of approximately −20 dB obtained from (61) (see also Figure 17-right). For other values of the parameter J_f the performance is even worst.

5.2 | QFT design of the dual-rate controller

The next design step consists of designing a QFT DR controller for the RWIP following the design procedure developed in Section 4. The fast controller (63) is used, jointly with the uncertain plant model and the design specifications (robust stability and robust tracking of a sinusoidal reference), to design a new slow controller, that will be referred to as $G_{L,QFT}$.

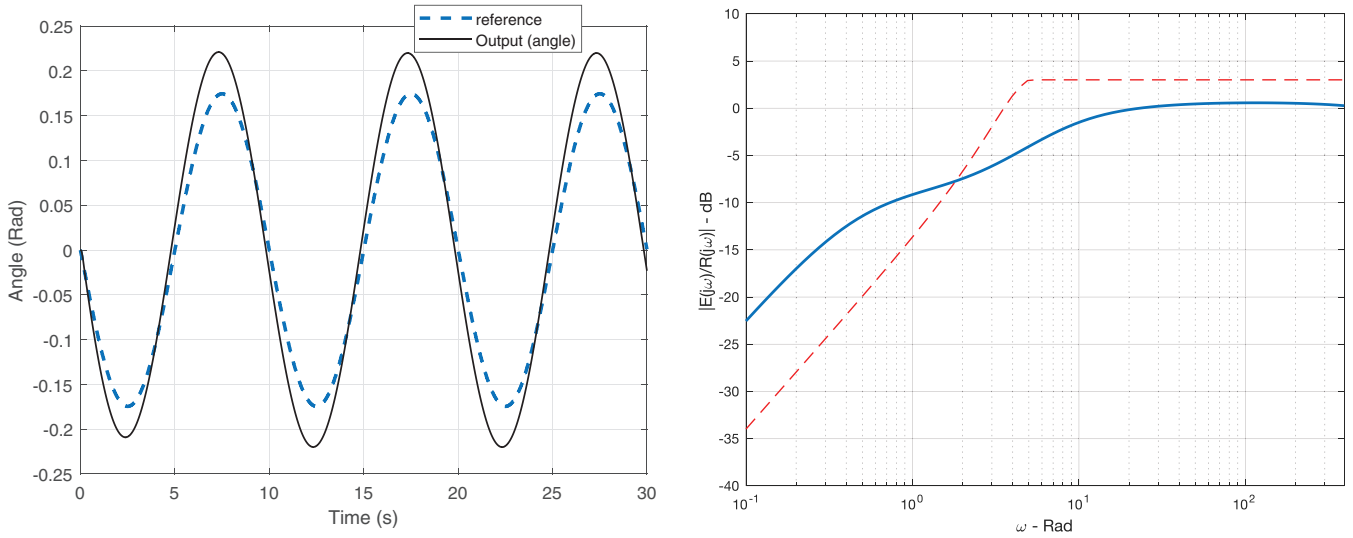

FIGURE 17 Tracking of a sinusoidal reference with the PID-based DR controller (62)–(63): left) RWIP angle (solid) and reference (dotted), and right) Sensitivity magnitude $|E(j\omega)/R(j\omega)|$ for the sinusoidal reference (solid), and tracking specification bound $\delta_2(\omega)$ (dotted)

Robust stability Note that the plant, given by (60), always have one unstable pole (the uncertain parameter J_f only affects its gain), thus the procedure developed in Section 4.1 (based on Proposition 1) can be directly used. DR control system stability is guarantied if: the nominal DR control system is stable, and the nominal open-loop gain is out of the forbidden regions defined by the stability bounds.

First, for stability of the nominal case Proposition 1 has to be used. Assumptions 1 and 2 are easily checked (details are omitted by brevity). This first stability condition is satisfied if the Nichols plot of the nominal open-loop gain makes a net number of crossings of $\mathbf{R}_0$ equal to 1 (the number of open-loop unstable poles). Since there is an open-loop integrator (given by (62)), then there is a half crossing $-1/2$ (see Remark 1). Thus, for a stable design with an open-loop integrator, the Nichols plot of the open-loop gain must perform a crossing $+1$ of the ray $\mathbf{R}_0$, in this way the net number of crossings is $-1/2+1=1/2$, and its double is the number of unstable poles. For example, the PID-based dual controller guaranties a nominal stable design (see Figure 18-left, its Nichols plot of the nominal open-loop gain satisfies the crossing condition). Note that the net number of crossings must be equal to $1/2$ for any nominal stable design.

Second, stability bounds are computed according to (45) for the stability margin $\mu=1/\sqrt{2}$ as specified. In this case, since there is only uncertainty in the gain plant all the stability bounds are identical for any frequency. The forbidden region corresponds to the shadow region in Figure 18-left. Note that, although the PID-based DR controller makes the nominal control system stable, its Nichols plot enters the forbidden region and thus the DR is not robustly stable with the specified margin. Thus, the slow controller must be redesigned to avoid the forbidden region at every frequency in order to satisfy design specifications.

Robust tracking Here, the design procedure starts with the computation the tracking bounds that define the forbidden regions in the Nichols plane. The chosen design frequencies are $\omega\in\{0.001,0.003,0.01,0.1,0.5,1\}\pi/T_s$. In this problem, frequencies beyond π/T_s result in forbidden regions that are not significative, since they are less demanding than for example the corresponding to stability bounds (details are omitted by brevity), and thus the design will be focused on frequencies below π/T_s. The computed stability bounds are shown in Figure 18-left. Note that the PID-based DR controller does not satisfy the tracking specifications for the design frequencies $0.001\pi/T_s$, $0.003\pi/T_s$, and $0.01\pi/T_s$.

Using the slow PID-based controller (62) as starting point, it needs to be redesign to satisfy both robust stability and tracking specifications. Clearly, its gain should be increased (this is equivalent to move upward the Nichols plot in Figure 18-left) to satisfy low frequencies bounds; however, something else is needed since otherwise high-frequency bounds may be crossed and thus tracking specifications would not be satisfied at those frequencies. A solution has been obtained both modifying the controller gain and its zero. The result is

$$G_{L,QFT}(z_s)=84.4\frac{z_s-0.9823}{z_s-1} \tag{64}$$

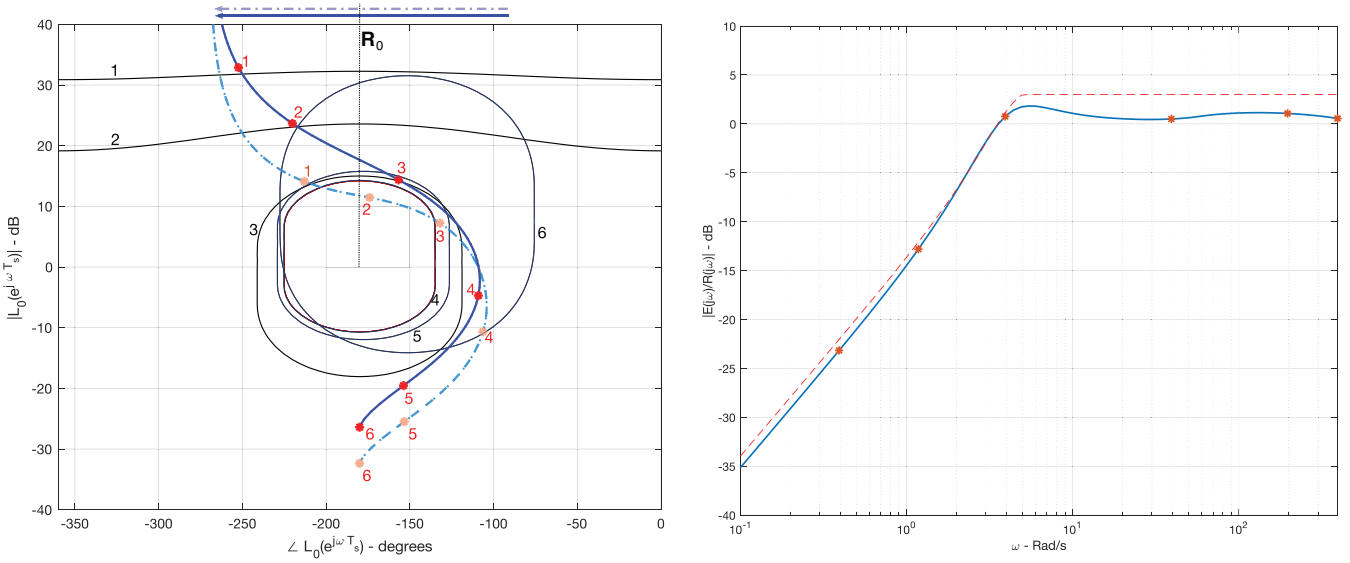

FIGURE 18 QFT design of the dual rate controller: (Left) stability and continuous-time tracking boundaries at $\omega \in \{0.001, 0.003, 0.01, 0.1, 0.5, 1\}\pi/T_s$, and loop-shaping of the PID-based DR controller (dashed), and the modified QFT controller (solid); (right) validation of robust continuous-time tracking specifications for the QFT design

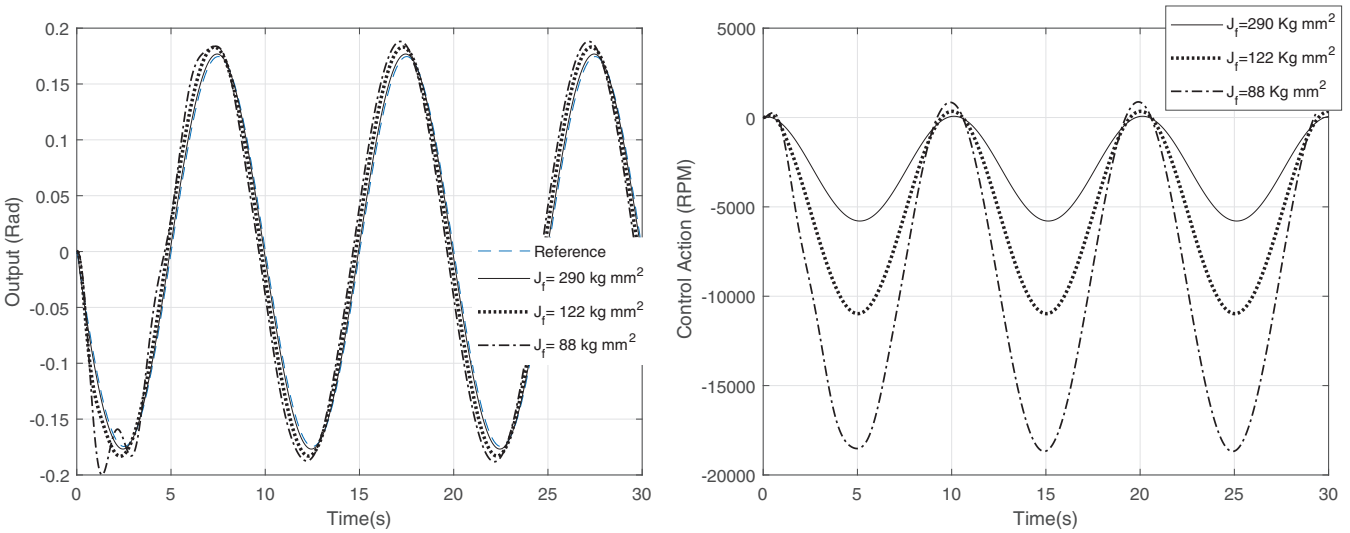

FIGURE 19 Tracking reference with QFT designed DR controller. Comparison among cases $J_f = 290$ kg mm^2, $J_f = 122$ kg mm^2, and $J_f = 88$ kg mm^2: (Left) Closed-loop output, (right) control action

Note that the Nichols plot of the open-loop gain corresponding to (64) satisfied the crossing condition, avoids the forbidden stability region, and also does not enters the forbidden regions defined by the tracking bounds. Regarding tracking, this must be validated for frequencies different to the design frequencies. Figure 18-right shows how the sensitivity function satisfies the tracking bound, and thus the design is validated.

Finally, time simulation plots with this new DR controller (63)–(64) are shown in Figure 19. The cases for $J_f = 290\,\text{kg}\,\text{mm}^2$ (nominal value), $J_f = 0.4 \times 290\,\text{kg}\,\text{mm}^2 = 122\,\text{kg}\,\text{mm}^2$, and $J_f = 0.3 \times 290$ kg mm^2 $= 88$ kg mm^2 (case without screws), have been considered. Note that the design performs correctly in spite of the uncertainty. As it may be expected, the design results in a more demanding control action of the motor for decreasing values of J_f.

6 | CONCLUSIONS

In spite of the large number of contributions on dual-rate control systems, there has been a lack of efficient techniques for their analysis and design in the frequency domain. In this work, a QFT approach is proposed to cope with this problem. Besides allowing the formulation a Nyquist-like stability result, also including worst-case stability margins, robust tracking specifications are considered both in the discrete-time domain and in the continuous-time domain. As a result, a new QFT-based technique has been developed for the design of robust DR control systems, using as a design element the slow discrete-time controller. Several detailed examples, and finally a case study (a reaction wheel inverted pendulum), have been developed including cases with/without uncertainty, and with continuous-time tracking specifications below/beyond the Nyquist frequency. To the authors knowledge, this work is the first interdisciplinary work on the areas of QFT and multirate control, that surprisingly have been isolated over the years. Throughout this work, several illustrative examples have been developed with a tutorial style, with the goal of building a bridge between both areas. The proposed approach is limited by several simplifying assumptions including the fact that the plant has a rational transfer function, and the fast and slow sampling rates are related by an integer. Overcoming these limitations will be investigated in future works.

ACKNOWLEDGMENTS

The work of A. Baños has been supported by Grant PID2020-112709RB-C22 funded by MCIN/AEI/ 10.13039/501100011033, and Grant 20842/PI/18 funded by Fundación Séneca (CARM); the work of J. Salt and V. Casanova under Grant RTI2018-096590-B-I00 funded by MCIN/AEI/ 10.13039/501100011033 and by "ERDF A way of making Europe".

CONFLICT OF INTEREST

The authors declare no potential conflict of interests.

AUTHOR CONTRIBUTIONS

The main contribution of this work is the development of a QFT framework for DR control systems having plants with potentially large uncertainty. It is mainly focused on the problem of robust stability and continuous-time tracking, and uses the slow-rate controller as design element. Several others performance specifications like disturbance rejection may be considered by using the developed framework. Some specific contributions are:

- The quantification of the closed-loop continuous-time response in the frequency domain under DR control, that will allow the efficient characterization of ripples, and in general of a desired intersample behavior.
- A Nyquist-like theorem for the robust stability of DR control systems, and the formulation of worst-case gain and phase margins, that results in QFT boundaries for the nominal slow open-loop gain function.
- Formulation of continuous-time tracking restrictions as QFT boundaries for the nominal slow open-loop gain function, for a given fast-rate controller and prefilter, with performance specifications below and beyond the slow Nyquist frequency.

As a result of the proposed approach, a number of new boundaries are developed that guaranty robust stability and continuous-time tracking. It is worthwhile to mention that this QFT approach can be also applied to design single-rate controllers with continuous-time specifications beyond the Nyquist frequency, extending previous work in the literature that suffered from that limitation. Also, it is useful for analyzing and designing DR controllers for plants with small or no uncertainty, although it is full potential is clearly obtained for the case of large uncertainty.

DATA AVAILABILITY STATEMENT

The data that support the findings of this study are available on request from the corresponding author. The data are not publicly available due to privacy or ethical restrictions.

ORCID

Alfonso Baños https://orcid.org/0000-0003-2711-4385

REFERENCES

1. Kalman RE, Bertram J. General synthesis procedure for computer control of single-loop and multiloop linear systems (An optimal sampling system). *Trans Am Inst Electr Eng II Appl Ind*. 1959;77(6):602-609.
2. Kranc G. Input-output analysis of multirate feedback systems. *IRE Trans Automat Contr*. 1957;3(1):21-28.
3. Jury EI. *Sampled-Data Control Systems*. Krieger Publishing Co., Inc; 1977.
4. Morant F, Albertos P. *Model Reference Control of a Cement Mill*. Elsevier; 1986:297-301.
5. Li D, Shah SL, Chen T, Qi KZ. Application of dual-rate modeling to CCR octane quality inferential control. *IEEE Trans Control Syst Technol*. 2003;11(1):43-51.
6. Hutchinson S. Multi-rate analysis and design of visual feedback digital servo-control system. *Urbana*. 1994;51:61801.
7. Sim T, Hong G, Lim K. Multirate predictor control scheme for visual servo control. *IEE Proc Control Theory Appl*. 2002;149(2):117-124.
8. Lozano-Perez T. *Autonomous Robot Vehicles*. Springer Science & Business Media; 2012.
9. Cuenca Á, Zhan W, Salt J, Alcaina J, Tang C, Tomizuka M. A remote control strategy for an autonomous vehicle with slow sensor using Kalman filtering and dual-rate control. *Sensors*. 2019;19(13):2983.
10. Cuenca Á, Salt J, Sala A, Pizá R. A delay-dependent dual-rate PID controller over an ethernet network. *IEEE Trans Ind Inform*. 2011;7(1):18-29.
11. Zhang D, Shi P, Wang QG, Yu L. Analysis and synthesis of networked control systems: a survey of recent advances and challenges. *ISA Trans*. 2017;66:376-392.
12. Alcaina J, Cuenca Á, Salt J, Zheng M, Tomizuka M. Energy-efficient control for an unmanned ground vehicle in a wireless sensor network. *J Sens*. 2019;2019:7085915. https://doi.org/10.1155/2019/7085915
13. Araki M, Hagiwara T. Pole assignment by multirate sampled-data output feedback. *Int J Control*. 1986;44(6):1661-1673.
14. Cimino M, Pagilla P. Design of linear time-invariant controllers for multirate systems. *Automatica*. 2010;46(8):1315-1319.
15. Salt J, Cuenca Á, Palau F, Dormido S. A multirate control strategy to the slow sensors problem: an interactive simulation tool for controller assisted design. *Sensors*. 2014;14(3):4086-4110.
16. Chen T, Qiu L. H^∞ design of general multirate sampled-data control systems. *Automatica*. 1994;30(7):1139-1152.
17. Sågfors MF, Toivonen HT, Lennartson B. H^∞ control of multirate sampled-data systems: A state-space approach. *Automatica*. 1998;34(4):415-428.
18. Lee JH, Morari M. Robust inferential control of multi-rate sampled-data systems. *Chem Eng Sci*. 1992;47(4):865-885.
19. Lall S, Dullerud G. An LMI solution to the robust synthesis problem for multi-rate sampled-data systems. *Automatica*. 2001;37(12):1909-1922.
20. Araki M, Yamamoto K. Multivariable multirate sampled-data systems: state-space description, transfer characteristics, and Nyquist criterion. *IEEE Trans Automat Contr*. 1986;31(2):145-154.
21. Araki M, Ito Y. Frequency-response of sampled-data systems I: open-loop consideration. *IFAC Proc Vol*. 1993;26(2):259-262.
22. Thompson PM. Gain and phase margins of multi-rate sampled-data feedback systems. *Int J Control*. 1986;44(3):833-846.
23. Salt J, Sala A. A new algorithm for dual-rate systems frequency response computation in discrete control systems. *Appl Math Model*. 2014;38(23):5692-5704.
24. Horowitz IM. *Quantitative Feedback Design Theory-QFT*. QFT Publications; 1993.
25. Horowitz IM. *Synthesis of Feedback Systems*. Academic Press; 1963.
26. Horowitz IM, Sidi M. Synthesis of feedback systems with large plant ignorance for prescribed time-domain tolerances. *Int J Control*. 1972;16(2):287-309.
27. Horowitz IM. A synthesis theory for linear time-varying feedback systems with plant uncertainty. *IEEE Trans Automat Contr*. 1975;20(4):454-464.
28. Horowitz IM. Synthesis of feedback systems with nonlinear time-varying uncertain plants to satisfy quantitative performance specifications. *Proc IEEE*. 1976;64:123-130.
29. Horowitz I, Baños A. *Advances in Nonlinear Systems. No. 264 in LNCIS*. Springer; 2001:63-134.
30. Baños A. Nonlinear quantitative feedbak theory. *Int J Robust Nonlinear Control*. 2007;17:181-202.
31. Yaniv O, Horowitz IM. A quantitative design method for MIMO linear feedback systems having uncertain plants. *Int J Control*. 1986;43(2):401-421.
32. Elso J, Gil-Martinez M, García-Sanz M. A quantitative feedback solution to the multivariable traking error problem. *Int J Robust Nonlinear Control* 2013; 24(16): 2331–2346.
33. Baños A, Horowitz IM. QFT design of multi-loop nonlinear control systems. *Int J Robust Nonlinear Control*. 2000;10(15):1263-1277.
34. García-Sanz M. *Robust Control Engineering: Practical QFT Solutions*. CRC Press; 2017.
35. Horowitz IM, Liao YK. Quantitative feedback design for sampled-data systems. *Int J Control*. 1986;44:665-675.
36. Yaniv O, Chait Y. Direct control design in sampled-data uncertain systems. *Automatica*. 1993;29(2):365-372.
37. Francis B, Georgiou T. Stability theory for linear time-invariant plants with periodic digital controllers. *IEEE Trans Automat Contr*. 1988;33(9):820-832.
38. Chen T, Francis B. Input-ouput stability of sampled-data systems. *IEEE Trans Automat Contr*. 1991;36(1):50-58.
39. Borghesani C, Chait Y, Yaniv O. *QFT Frequency Domain Control Design Toolbox*. Terasoft; 2000.
40. Gutman PO. Qsyn: the Toolbox for robust control systems design for use with Matlab; 1996.
41. García-Sanz M. The QFT control toolbox (QFTCT) for Matlab; 2008.
42. Rubin D, Gutman P. *Open Qsyn*. 2019. https://qsyn.github.io

43. Chait Y, Chen Q, Hollot CV. Automatic loop-shaping of QFT controllers via linear programming. *J Dyn Syst, Measur Control*. 1999;121(3):351-357.
44. García-Sanz M, Guillen JC. Automatic loop-shapping of QFT robust controllers via genetic algorithms; 2000.
45. Nataraj PSV, Kubal N. Automatic loop shaping in QFT using hybrid optimization and constraint propagation techniques. *Int J Robust Nonlinear Control*. 2006;17:251-264.
46. Cervera J, Baños A. Automatic loop shaping in QFT using CRONE structures. *J Vib Control*. 2008;14(9):1513-1529.
47. Braslavsky JH. *Frequency-Domain Analysis of Sampled-Data Control Systems*. The University of Newcastle; 1995.
48. Eitelberg E. Quantitative feedback design for tracking error tolerance. *Automatica*. 2000;36:319-326.
49. Boje E. Pre-filter design for tracking error specifications in QFT. *Int J Robust Nonlinear Control*. 2003;13:637-642.
50. Sklansky J, Ragazzini J. Analysis of errors in sampled-data feedback systems. *Trans Am Inst Electr Eng II Appl Ind*. 1955;74(2):65-71.
51. Coffey TC, Williams IJ. Stability analysis of multiloop, multirate sampled systems. *AIAA J*. 1966;4(12):2178-2190.
52. Khargonekar P, Poolla K, Tannenbaum A. Robust control of linear time-invariant plants using periodic compensation. *IEEE Trans Automat Contr*. 1985;30(11):1088-1096.
53. Bamieh B, Pearson J, Francis B, Tannenbaum A. A lifting technique for linear periodic systems with applications to sampled-data control. *Syst Control Lett*. 1991;17(2):79-88.
54. Whitbeck RF, Didaleusky D. Multirate digital control systems in simulation applications. Report AFWAL-TR-80-3101, Vols. I, II and III; 1980.
55. Salt J, Alcaina J. Dual-rate sampled-data systems. some interesting consequences from its frequency response analysis. *Int J General Syst*. 2019;48(5):554-574.
56. Salt J, Sala A. A new algorithm for dual-rate systems frequency response computation en discrete control systems. *Appl Math Model*. 2014;38:5692-5704.
57. Salt J, Albertos P. Model-based multirate controllers design. *IEEE Trans Control Syst Technol*. 2005;13(6):988-997.
58. Keller JP, Anderson BD. A new approach to the discretization of continuous-time controllers; 1990:1127-1132; IEEE.
59. Er MJ, ANDERSON BD. Practical issues in multirate output controllers. *Int J Control*. 1991;53(5):1005-1020.
60. Dasgupta S. An approach to multirate control. Proceedings of the 38th IEEE Conference on Decision and Control; 1999:3446-3451.
61. Cohen N, Chait Y, Yaniv O, Borghesani C. Stability analysis using Nichols charts. *Int J Robust Nonlinear Control*. 1994;4(1):21-46.
62. Chen WH, Ballance DJ. Stability analysis on the Nichols chart and its application in QFT. Technical report CSC-98013, Center for Systems and Control, University Glasgow; 1998.

How to cite this article: Baños A, Salt J, Casanova V. A QFT approach to robust dual-rate control systems. *Int J Robust Nonlinear Control*. 2022;32(2):1026-1054. doi: 10.1002/rnc.5861